DESIGN AND VERIFICATION OF THE AIRCRAFT CONFLICT PREDICTION AND RESOLUTION ALGORITHMS

by

Arnab Nilim

Memorandum No. UCB/ERL M01/18

25 January 2001

DESIGN AND VERIFICATION OF THE AIRCRAFT CONFLICT PREDICTION AND RESOLUTION ALGORITHMS

by

Arnab Nilim

Memorandum No. UCB/ERL M01/18

25 January 2001

ELECTRONICS RESEARCH LABORATORY

College of Engineering
University of California, Berkeley
94720

Design and Verification of the Aircraft Conflict Prediction and Resolution Algorithms

Arnab Nilim
Department of Electrical Engineering and Computer Sciences
University of California, Berkeley
Berkeley, CA 94720, USA
nilim@eecs.berkeley.edu

Design and Verification of the Aircraft Conflict Prediction and Resolution Algorithms

Arnab Nilim

Research Report

Submitted to the Department of Electrical Engineering and Computer Sciences, University of California at Berkeley, in partial fulfilment of the requirements for the degree of **Master of Science, Plan II**

Approval for the report and Comprehensive examination:
Committee:

05/01/01

Prof. S. Shankar Shastry, Research Adviser — Date

2/05/01

Prof. Laurent El Ghaoui, Second Reader — Date

Abstract

Conflict detection and conflict resolution schemes are proposed. Conflict detection is based on a measure of criticality which directly takes into account the uncertainty in the prediction of the aircraft positions. The use of randomized algorithms makes the computation of the criticality measure tractable. The performance of the algorithm is evaluated by Monte Carlo simulation on a stochastic ODE model of the aircraft motion. Conflict resolution deals with situations involving multiple aircraft. Energy of maneuvers is then used as cost function for choosing among all conflict-free joint maneuvers the optimal one. As for the multiple aircraft case, an approximate solution to the constrained optimization is proposed which consists of finding the optimal two-legged joint maneuver by solving a convex optimization problem for each type of maneuver. Inclusion of velocity and way-point constraints induces nonlinearity in the constraint set. Second order cone programming (SOCP) is used to solve the problem. A 3-D extension of the resolution algorithm is presented. Finally, simulation results are presented for some typical multi-aircraft encounters for both the 2-D and the 3-D cases.

Dedicated To my Mother

Acknowledgments

The author wishes to express his sincerest debt of gratitude to Professor Shankar Sastry for his continuous guidance, valuable suggestions and generous help at all stages of this endeavor. It was a pleasant and valuable experience to work with him.

The author also wants to express his extreme gratitude to Professor Elghaoui for his kind guidance and tutelage in the research relating to the convex optimization techniques and his willingness to be the second reader for this report.

The author would like to thank his co-workers Maria, Jianghai and John for their constant support and encouragement.

Finally, special thanks goes to Tony, Mekhail and Kiran who have made Berkeley his home away from home.

Research supported in part by NASA under grant NAG 2-1038 and the FAA Center of Excellence, NEXTOR.

Contents

Chapter 1

Overview

Air travel is in great demand in the United States. Each year, hundreds of millions of passengers are flown all over the country. Although the airline industry originated more than 50 years ago, it is still a growth industry, with a rate of increase faster than the growth rate of the nation's gross national product (GNP). Moreover, air transportation is expected to maintain its dominant position since no projected mode of transportation can replace it from its own market. Because so many people are flying so frequently, the airports and airways of the United States are no longer adequate to move them smoothly to their proffered destinations. It is difficult to state with precision the dollar amount of damages caused by delay due to congestion, but it can be estimated to be around 15 billion US dollars. In spite of tremendous technological advancement, current the Air traffic management system uses technologies that were developed at least a decade back. Adding physical facilities in the airport, i.e., runways, taxiways, is very expensive and many times, is limited by geographic and political constraints. Recent technological advances, such as on-board computing facilities and Global Positioning Satellite System (GPS) can help us to automate the system for efficient control, scheduling and landing of larger numbers of aircraft. In addition, it is imperative to reduce the controller's work load with this automated system and to give more autonomy to the individual aircraft. The concept of free flight is proposed [5]. Free flight is an innovative concept designed to enhance the safety and efficiency of the National Airspace System (NAS). The concept moves the NAS from a centralized command-and-control system between pilots and air traffic controllers to a distributed system that allows pilots, whenever practical, to choose their own route and file a flight plan that follows the most efficient and economical route. Free flight calls for limiting pilot flexibility in certain situations, such as : to ensure separation at high-traffic airports and in congested airspace, to prevent unauthorized entry into special use airspace, and for any safety reasons. The free flight is described in the hierarchal and hybrid control framework [19].

The principle of maintaining safe airborne separation is at the center of the free flight concept. This principle is based on two airspace zones, protected and alert, the sizes of which are based on the aircraft's speed, performance characteristics, and communications, navigation, and surveillance equipment. The protected zone, the one closest to the aircraft, can never meet the protected zone of another aircraft. The alert zone extends well beyond the protected zone, and aircraft can maneuver freely until alert zones touch. If alert zones do touch, a controller may provide one or both pilots with course corrections or restrictions

to ensure separation. Eventually, most commands will be sent via data link, an integrated network of air, ground, and airborne communications systems. Additionally, on-board computers and Global Positioning System satellites will allow pilots, with the concurrence of controllers, to use airborne traffic displays to choose solutions. So we can define conflict as a situation where two aircraft come within 5 n.mi (each other's protected zone) of one another horizontally and within 1000 ft or 2000 ft vertically depending on whether the flight level is below or above 29000 ft [16]. Our purpose is to come up with an efficient and accurate conflict detection and resolution algorithm. There has been a handful of research work done in this field [11]. Most of the comprehensive work has been done in the deterministic setting [21]. In this presentation, we will introduce a probabilistic conflict detection and resolution scheme. If the initial and destination positions, flight plans and scheduled times of arrival to those points are given, the probability that two or more aircraft will be in conflict as defined above is estimated. If the probability of conflict is higher than a threshold value, some control is needed to avoid the conflict. In the resolution stage, we will replan the trajectories of the aircraft involved in conflict such that the probability of conflict goes below the threshold probability. In the resolution stage, we have also taken efficiency into consideration. We have optimized the new trajectories such that the deviation from the nominal path is minimized.

There are three parts in this report. Chapter 2 of the paper deals with the probabilistic conflict detection. The schemes proposed here make extensive use of randomized algorithms for estimating integrals and carrying out optimizations. The advantage of the randomized techniques is that they tend to be computationally more efficient. They also provide the analytic bounds on the accuracy of the approximation involved, provided one makes appropriate design choices. The cost functions for conflict resolution is an example of the design choice. We provide the probabilistic scheme and perform the validation. We also describe how to deal with the involved computational issues in order to formulate the algorithmic version of the proposed scheme. Finally, the monte carlo simulation results obtained through the proposed validation model are reported in this chapter.

In chapter 3, we have studied the conflict resolution problem where multiple aircraft are involved in a potential conflict in the 2 dimensional case. Similar to [3],[6], our approach to multiple aircraft conflict resolution is based on the optimization of a cost function, which is suitably chosen to take into account practical factors such as passenger comfort, in addition to being conflict free. The problem is formulated as a finite dimensional optimization problem, by parameterizing the resolution maneuvers by means of a finite number of variables. We used the notion of energy as in [10] in order to find the optimal resolution maneuver among the conflict free zones. Thus the problem is to find the trajectories which will provide the minimum cost. We have also added further constraints on the way-points for the maneuver feasibility. The constraints are velocity constraints and the turning angle constraints. Addition of these constraints induces non linearity in the constraint set. We have used the Second-order cone programming (SOCP) techniques to solve this quadratic constraints problem. In chapter 4, we study the problem of finding optimal three dimensional conflict-free maneuvers for multiple aircraft. As this is a 3-D problem, there are more degrees of freedom in the optimization problem. The change of altitude is the additional maneuver which arises due to increased dimension. We minimize a certain energy function to obtain the most efficient conflict-free maneuvers. A priority mechanism is incorporated into the cost function so that aircraft with lower priority assume more responsibility in resolving the

conflicts. Moreover, vertical maneuvers are penalized with respect to horizontal ones for the sake of passenger comfort. A geometric construction and a numerical algorithm are given to determine the optimal maneuver in the two aircraft case. As for the multi-aircraft case, an approximation scheme is proposed to compute a suboptimal two-legged solution. We have also added the velocity and the way-point constraints in the optimization problem in order to get a more practical solution. SOCP is used here to solve the optimization problem.

Chapter 2

Probabilistic aircraft conflict detection and validation

2.1 Introduction

Air traffic control(ATC) is a safety critical system. The main objective of deriving the algorithms for Aircraft conflict detection and resolution is to ensure safety and efficiency of the ATC system. Aircraft conflict detection and resolution requires attention be given at three different levels of the air traffic management process.

1. Long range: Some form of conflict prediction and resolution is carried out at the level of the entire National Airspace System (NAS), over a horizon of several hours. It involves composing flight plans and airline schedules (on a daily basis, for example) to ensure that airport and the sector capacities are not exceeded. This is typically accomplished using large scale integer and linear programming techniques [1],[23]

2. Mid-Range: Conflict prediction and resolution is carried out by ATC, over horizons of the orders of ten minutes. It involves modifying the pre-planned flight plan on-line, to ensure adequate separation. Algorithm in [12],[20], [4] operate in this level.

3. Short range: Conflict prediction and resolution is also carried out on board the aircraft, over horizons of seconds to minutes. this is typically considered as a last resort solution. The Traffic alert and Collision Avoidance System (TCAS) currently operating on all commercial aircraft is such a prediction/resolution algorithm (as in [5],[14]).

The work presented here concentrates primarily on the midrange level of the air traffic management process [17],[18]. It is assumed that the proposed algorithms will eventually be implemented as computational tools to provide assistance to ATC.

The ATC process and its interaction with the conflict detection and prediction is summarized in fig1. ATC and its components are are arranged in a feedback loop. The ATC, aircraft and radar correspond to the plant while the prediction and resolution components correspond to the controller. Our goal is to design the "Controller" modules and verify that the closed loop system possesses certain desirable properties (safety, ATC workload, Efficiency, Less delay etc).In this chapter, we present a randomized algorithm for the conflict

detection which is computationally more efficient. They also provide the analytical bounds on the accuracy of the approximation involved with an intelligent design choices.

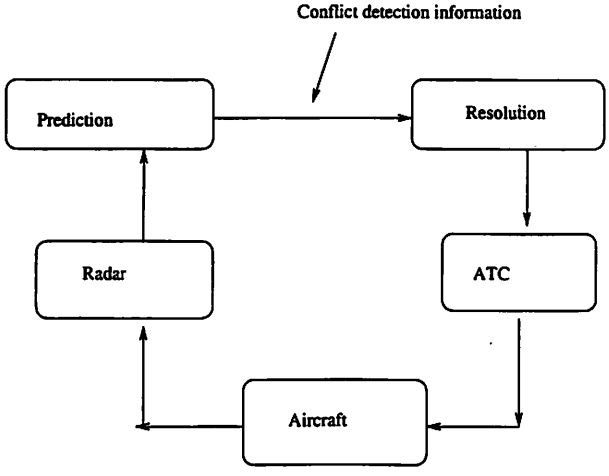

Figure 2.1: Outline of the conflict prediction/resolution functionality

Validation of the prediction scheme requires one to model the radar and the aircraft. Here we use a simple model for the radar (additive white noise) and we introduce a stochastic difference equation to model the aircraft movement. Validation of the detection scheme is then carried out by the Monte carlo simulation.

2.2 Probabilistic Models

2.2.1 Flight Plans and Configuration

Consider N_a aircraft sharing a region of the airspace. Assume that the *flight plan* of aircraft i consists of a sequence of *way points*, $\{P_j^i\}_{j=0}^{n_i}$, $P_j^i \in \Re^3$, given in a global coordinate frame, and a sequence of *speeds*, $\{v_j^i\}_{j=1}^{n_i}$, $v_j^i \in \Re_+$. The interpretation is that aircraft i follows the sequence of way points, moving roughly along the straight line joining successive way points P_{j-1}^i and P_j^i with velocity v_j^i. P_0^i and $P_{n_i}^i$ respectively represent the current position of aircraft i (available through ADSB or radar) and the threshold of the landing runway at the destination airport. The *nominal time of arrival* of aircraft i at way point j can be recursively computed by $T_j^i = \|P_j^i - P_{j-1}^i\|/v_j^i + T_{j-1}^i$, $j > 0$, with $T_0^i = 0$. Likewise, the *nominal distance traveled* by aircraft i, $s^i(t) \in \Re$, and its *nominal position*, $p^i(t) \in \Re^3$, at time $t \in (T_{j-1}^i, T_j^i]$, can be respectively computed by $s^i(T_0^i) = 0$, $s^i(t) = v_j^i(t - T_{j-1}^i) + s^i(T_{j-1}^i)$, and $p^i(t) = P_{j-1}^i + v_j^i(t - T_{j-1}^i)\frac{P_j^i - P_{j-1}^i}{\|P_j^i - P_{j-1}^i\|}$.

The *configuration*, γ, of the N_a aircraft system consists of the flight plans of all aircraft, $\gamma = \left\{\{P_j^i\}_{j=0}^{n_i}, \{v_j^i\}_{j=1}^{n_i}\right\}_{i=1}^{N_a}$. We assume that the flight plan of each aircraft is known, except of course the way point encoding the current position, which depends on how well the aircraft is tracking the flight plan. The models introduced below assume that an aircraft turns instantaneously and heads for the new way point at the scheduled time, even if it has deviated from its flight plan. This assumption is somewhat unrealistic, but is used in the

prediction model to simplify the computation. It can be easily relaxed for the validation model, if better models for the way aircraft execute turns become available.

2.2.2 Prediction model

The actual position of the aircraft is affected by uncertainty, due to wind and errors in tracking, navigation, and control. Following [16, 12], we assume that the *predicted position* $x^i(t) \in \Re^3$, of aircraft i can be modeled as a multivariate Gaussian random variable, $x^i(t) \sim N(p^i(t), Q^i(t))$, independent of the random variables modeling the positions of other aircraft. Notice that the mean is equal to the nominal position of aircraft i along its flight plan. The variance of the predicted position is assumed to increase with time, reflecting the fact that the uncertainty about the position of the aircraft increases the further we try to predict into the future. In [16], a distinction is made between the variances in the *along track* and *cross track* directions. It is assumed that the standard deviation of the along track component grows linearly with time:

$$\sigma^i_{AT}(t) = c_1 + c_2 t.$$

The standard deviation of the horizontal cross track component, grows linearly with the distance traveled and then saturates at a fixed value:

$$\sigma^i_{CTH}(t) = \min\{c_4, c_1 + c_3 s^i(t)\}.$$

Finally, the standard deviation of the vertical cross track component, remains constant:

$$\sigma^i_{CTV}(t) = c_5.$$

The values $c_1 = 50/1850$ *nmi*, $c_2 = 0.25$ *nmi/min*, $c_3 = 1/57$, $c_4 = 1$ *nmi*, and $c_5 = 30/1850$ *nmi* were proposed in [16, 11], based on empirical air traffic data. Since the uncertainty components are assumed to be independent, the covariance matrix for $t \in [T^i_{j-1}, T^i_j)$ is given by:

$$Q^i(t) = R \begin{bmatrix} (\sigma^i_{AT})^2(t) & 0 & 0 \\ 0 & (\sigma^i_{CTH})^2(t) & 0 \\ 0 & 0 & (\sigma^i_{CTV})^2(t) \end{bmatrix} R^T$$

where we set $R \in SO(3)$ for the rotation matrix $R(\theta^i_j, \phi^i_j)$ associated with the angles θ^i_j and $\pi/2 - \phi^i_j$ that the vector $P^i_j - P^i_{j-1}$ makes with the x_1 and x_3 axes of the global coordinate frame in which the P^i_j's are given.

This model is fairly accurate for mid-range conflict prediction, as it reflects the fact that pilots tend to correct cross track errors in the short term and deal with along track errors in the long term, using small changes in speed [16]. The accuracy of the model is limited by the assumption that the positions of the aircraft are uncorrelated. Since the tracking noise is primarily due to wind, the positions of the aircraft may in fact be correlated, especially near the conflict point where they are close one to the other. We are currently investigating ways of relaxing this assumption.

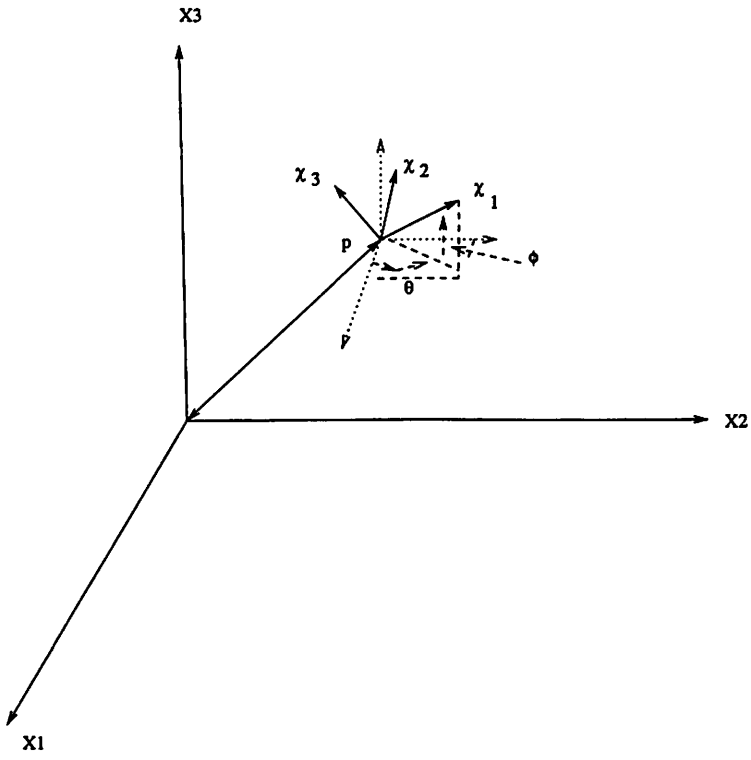

Figure 2.2: The body and inertial frames.

2.2.3 Validation model

The prediction model is simple and allows fast computations, but has inherent limitations, which limit its applicability for simulation and validation. To remove some of these limitations we introduce a stochastic ODE model and use it to generate aircraft trajectories for validation. The validation model provides a formal way of correlating the positions of a single aircraft at different points in time.

Consider an aircraft moving in $\Re^3$, and let x denote its position with respect to a global inertial coordinate frame. Assume its velocity has magnitude v and makes an angle θ with respect to the x_1 axis and $\pi/2 - \phi$ with respect to the x_3 axis. Consider a body coordinate frame $\chi = [\chi_1\ \chi_2\ \chi_3]^T$ with χ_1 aligned with the aircraft velocity (along track), χ_2 perpendicular to it and lying on the plane on which the aircraft flies (cross track horizontal), and χ_3 perpendicular to χ_1 and χ_2 (cross track vertical) (Figure 1). The two frames are related through the coordinate transformation

$$x = R(\theta, \phi)\chi + p, \tag{2.1}$$

where $R(\theta, \phi)$ is the rotation matrix and p denotes the position of the origin of the body frame with respect to the inertial frame. p can be interpreted as the nominal position of the aircraft, x as its actual position, and χ as the variation of the aircraft position with respect to the nominal one along the tracking directions.

The nominal position p evolves according to:

$$\dot{p} = R(\theta, \phi)[1\ 0\ 0]^T v \tag{2.2}$$

We assume that the uncertainty in the position around the nominal point is obtained through the ODE:

$$\dot{\chi} = A\chi + \eta \tag{2.3}$$

where $\chi(0) \sim N(0, V_\chi(0))$ and $\eta \in \Re^3$ is a white Gaussian noise $\eta(t) \sim N(0, V_\eta(t))$ independent of $\chi(0)$. Combining equations (2.1)-(2.3) produces the kinematic model

$$\begin{cases} \dot{x} = [(\frac{\partial R}{\partial \theta}\omega_\theta + \frac{\partial R}{\partial \phi}\omega_\phi)R^T + RAR^T](x-p) \\ \qquad +R[1\ 0\ 0]^T v + R\eta, \\ \dot{p} = R[1\ 0\ 0]^T v, \qquad \dot{\theta} = \omega_\theta, \qquad \dot{\phi} = \omega_\phi \end{cases}$$

where $(v, \omega_\theta, \omega_\phi)$ are the linear and angular velocities.

The above equations describing the aircraft motion are nonlinear. To make them linear we can adopt the simplification $\omega_\theta \equiv \omega_\phi \equiv 0$, and model turns as discrete events occurring at the way points. This leads to a piecewise linear stochastic ODE: for $t \in [T_{j-1}, T_j)$,

$$\begin{cases} \dot{x} = A(\theta_j, \phi_j)(x-p) + B(\theta_j, \phi_j)v_j + C(\theta_j, \phi_j)\eta \\ \dot{p} = D(\theta_j, \phi_j)v_j, \end{cases}$$

where $A(\theta, \phi) = RAR^T$, $C(\theta, \phi) = R$, and $B(\theta, \phi) = D(\theta, \phi) = R[1\ 0\ 0]^T$. The initial conditions are $p(0) = P_0$ and $x(0) \sim N(P_0, R(\theta_1, \phi_1)V_\chi(0)R(\theta_1, \phi_1)^T)$, independent of the white Gaussian noise $\eta \sim N(0, V_\eta(t))$. The initial conditions and the noise processes for different aircraft are assumed to be independent.

Position estimates $y \in \Re^3$ for each aircraft are obtained every Δ seconds through radar measurements (typically $\Delta = 12$). We set

$$y(k\Delta) = x(k\Delta) + \xi(k\Delta),$$

where the noise $\{\xi(k\Delta)\}_{k\geq 0}$ is described as a sequence of i.i.d. Gaussian random variables with $\xi(k\Delta) \sim N(0, V_\xi)$ and it is independent of all the other random variables involved in the validation model.

For our stochastic validation model to resemble the statistics derived from air traffic data, we need to appropriately choose $V_\chi(0)$, $V_\eta(t)$, A and V_ξ. For the radar model parameters, we set $V_\xi = diag(V_{\xi_1}, V_{\xi_2}, V_{\xi_3})$ where $V_{\xi_1} = V_{\xi_2} = c_1^2$ and $V_{\xi_3} = c_5^2$, to reproduce the statistical characteristics described in [16] for the uncertainty in the current aircraft position. For the aircraft model we set $V_{\chi_1}(0) = V_{\chi_2}(0) = c_1^2$, $V_{\chi_3}(0) = c_5^2$, $V_{\eta_1}(t) = 2c_1c_2 + 2c_2^2 t$, $V_{\eta_2} = 2a_2c_4^2$, $V_{\eta_3} = 2a_3c_5^2$, where $A = diag(0, -a_2, -a_3)$, $a_2 = \frac{c_3}{(c_4 - c_1)}v_1$ and $a_3 = 1\ nmi^{-1}$. From standard results in stochastic linear systems , $\chi_1(t)$, $\chi_2(t)$, and $\chi_3(t)$ will then be independent, zero mean Gaussian random variables, with

$$\begin{aligned} var[\chi_1(t)] &= (c_1 + c_2 t)^2 \\ var[\chi_2(t)] &= c_4^2 + [c_1^2 - c_4^2]e^{-\frac{2c_3}{(c_4-c_1)}v_1 t} \\ var[\chi_3(t)] &= c_5^2 \end{aligned}$$

χ_1 and χ_3 are Gaussian processes exactly matching the mean and variance characteristics of the along track and vertical cross track errors. The time constant of the exponential for the Gaussian process χ_2 is equal to 1/2 of the time $\bar{t} = \frac{c_4 - c_1}{c_3 v_1}$ required for $\sigma^2_{CTH}(t)$ to reach the

saturation value c_4^2 in the case when the aircraft trajectory is a straight line traveled with speed v_1. For typical speeds ($v_1 = 500\ nmi/h$), $var[\chi_2(t)]$ reaches 86% of the saturation value in about 6 minutes. Ideally, the value of a_3 should be set based on the estimate of the correlation between the aircraft positions at different time instants, as it does not affect any other relevant statistics. Since this piece of information is not available in the literature, we arbitrarily set it equal to 1 nmi^{-1}.

2.3 Conflict Detection

2.3.1 General Conflict Detection

The desired separation among aircraft is typically encoded by means of a minimum *horizontal separation*, d_H, and a minimum *vertical separation*, d_V. Currently $d_H = 5\ nmi$ for en-route airspace and 3 nmi in the TRACON, and $d_V = 2000\ ft$ above 29000 ft and 1000 ft below 29000 ft. The *conflict set* is then given by $C = \{(u_1, u_2, u_3) \in \Re^3 : (u_1^2 + u_2^2 \leq d_H^2) \wedge (|u_3| \leq d_V)\}$.

Conflict detection consists of extracting some measure, $C(\gamma)$, of how safety critical the current configuration, γ, is, comparing this measure to a threshold, P, and declaring a conflict if P is exceeded. The process should be repeated every time γ changes, that is when a new measurement comes in from the radar, the ATC changes a flight plan, etc.

Algorithm for general Conflict Detection
when γ changes **do**
Compute $C(\gamma)$
if $C(\gamma) > P$ declare a conflict
end

In this paper we use the maximum of the probability of conflict over a horizon T as a measure of criticality[1]. Consider two aircraft, 1 and 2, let x^1 and x^2 denote their positions in the inertial reference frame. Given the probability density function $f(u,t)$ for the separation $u(t) = x^1(t) - x^2(t)$ of the two aircraft at time t, the probability of conflict at time t is given by

$$PC(t) = Prob(u \in C) = \int_C f(u,t)du.$$

For the prediction model, the predicted separation of two aircraft at time t is a Gaussian random variable with mean $\mu(t) = p^1(t) - p^2(t)$ and covariance matrix $Q(t) = Q^1(t) + Q^2(t)$. We set $C(\gamma) = \sup_{t\in[0,T]} PC(t)$, and, following [16], $T = 20$ minutes.

The major obstacle in the implementation of Algorithm 1 is the computation of $C(\gamma)$, since one can not derive an analytical expression for $PC(\cdot)$. In the literature techniques for estimating $C(\gamma)$ have been proposed using Monte Carlo simulation [12] and analytical approximation [16]. We propose an algorithm for approximating $C(\gamma)$ based on the theory of empirical processes [22].

[1]Other measures of criticality (such as weighted averages of the probability of conflict) were also tested as part of this study and were found to be less effective than the maximum.

2.3.2 Estimation of $C(\gamma)$

Suppose for the time being that we are able to compute $PC(t)$ with no error. Let $\mathcal{Q}$ be the uniform distribution on $[0,T]$, and consider the following algorithm for computing an estimate, $C'(\gamma)$, of $C(\gamma)$.

Algorithm for Randomized Estimate of $C(\gamma)$
Choose an integer N and set $C'(\gamma) = 0$
for $i = 1, \ldots, N$
Extract $t_i \in [0,T]$ according to $\mathcal{Q}$
if $C'(\gamma) < PC(t_i)$ **then** $C'(\gamma) = PC(t_i)$
end

Clearly, $C'(\gamma) = \max_{t \in \{t_i\}_{i=1}^N} PC(t) \leq C(\gamma)$, since we are testing just N values of $PC(t)$. In addition, the quality of the approximation is random due to the stochastic selection of the t_i's. Nevertheless, if the random extractions are independent, it can be shown that C' is a good approximation in a probabilistic sense.
Theorem for the Estimation of $C(\gamma)$: Fix $\beta > 0$ and consider the probability space $([0,T], \mathcal{F}, \mathcal{Q})$ where $\mathcal{F}$ is the Borel σ-algebra on $[0,T]$.
Then

$$\mathcal{Q}\{t \in [0,T] : PC(t) > C'(\gamma)\} \leq \beta \tag{2.4}$$

with probability greater than $1 - (1-\beta)^N$.

In other words, if we set $N = \lceil \frac{\ln(\delta)}{\ln(1-\beta)} \rceil$ (where $\lceil z \rceil$ denotes the smallest integer greater than z), there exists an exceptional $S \subset [0,T]$ of Lebesgue measure at most βT such that $\sup_{[0,T]\setminus S} PC(t) \leq C' \leq \sup_{[0,T]} PC(t)$ with probability at least $1 - \delta$. Hence, C' is an approximation of C in the sense that is bracketed by the supremum of $PC(t)$ over all $[0,T]$ and the supremum of $PC(t)$ over "nearly" all of $[0,T]$ with high probability.

2.3.3 Estimation of $PC(t)$

Next, we introduce a method for computing a uniformly good approximation of $PC(t)$ over a finite set of time instants $\{t_1, t_2, \ldots, t_N\}$. Recall that $PC(t)$ is the measure of the fixed set $\mathcal{C}$ according to $N(\mu(t), Q(t))$. By an appropriate change of coordinates, however, it can also be viewed as the measure of a time dependent set, $\mathcal{C}_t$, according to the standard normal distribution $N(0, I)$. The required change of coordinates can be found by computing the Cholesky factorization[2] $Q(t) = L(t)L(t)^T$ of the covariance matrix, and setting $w = L(t)^{-1}[u - \mu(t)]$. We then get $PC(t) = \int_{\mathcal{C}_t} \frac{1}{2\pi} e^{-\frac{1}{2}w^T w} dw$, where $\mathcal{C}_t = \{w \in \Re^3 \ : \ L(t)w + \mu(t) \in \mathcal{C}\}$. This suggests the following algorithm for probabilistically estimating $PC(t)$.

Theorem for the randomized Estimate of $PC(t)$
Choose an integer M and set $PC'(t) = 0$
for $j = 1, \ldots, M$ **do**

[2] A similar procedure is followed in [16].

Extract $w_j \in \Re^3$ according to $N(0, I)$
$PC'(t) = PC'(t) + I_{w_j \in C_t}$
end
$PC'(t) = \frac{PC'(t)}{M}$

$I_{\text{expression}}$ denotes the indicator function. Again, $PC'(t) = \frac{1}{M} \sum_{j=1}^{M} I_{w_j \in C_t}$ is a random approximation of $PC(t)$, due to the stochastic selection of the w_j's. Under the assumption that the random extractions are independent, the following result quantifies the level of approximation involved.

Theorem for the Estimation of PC
Fix $\epsilon \in (0, 1)$ and consider the probability space $(\Re^3, \mathcal{F}, N(0, I))$ where $\mathcal{F}$ is the Borel σ-algebra on $\Re^3$. Then,

$$N^M\{w^M \in \Re^{3M} : \sup_{t \in \{t_i\}_{i=1}^N} |PC'(t_i) - PC(t_i)| > \epsilon\} \leq 2Ne^{-2M\epsilon^2}$$

where w^M denotes $(w_1, w_2, \ldots, w_M)$.

Hence, each finite collection of sets $\{C_{t_i}\}_{i=1}^N$ has the property of uniform convergence of empirical probabilities since for each fixed ϵ the estimates uniformly convergences to their true values as the number of samples M goes to infinity.

2.3.4 Randomized Conflict Detection

The following algorithm brings the two procedures together.

Algorithm for the Randomized Conflict Detection
Fix $P \in [0,1]$ and ϵ, β, and $\delta \in (0,1)$
Set $N = \lceil \frac{\ln(\frac{\delta}{2})}{\ln(1-\beta)} \rceil$, $M = \lceil \frac{1}{2\epsilon^2} \ln \frac{4N}{\delta} \rceil$
when γ changes **do**
Extract $w_j \in \Re^3$, $j = 1, \ldots, M$ according to $N(0, I)$
Extract $t_i \in [0, T]$, $i = 1, \ldots, N$ according to $\mathcal{Q}$
for $i = 1, \ldots, N$ **do**
Compute $\mu(t_i)$ and $Q(t_i)$
Compute $Q(t_i) = L(t_i)L(t_i)^T$
$PC'(t_i) = 0$
for $j = 1, \ldots, M$ **do**
$PC'(t_i) = PC'(t_i) + I_{w_j \in C_{t_i}}$
end
$PC'(t_i) = \frac{PC'(t_i)}{M}$
if $PC'(t_i) > P$ declare a conflict
end
end

A conflict is declared if and only if the estimate

$$C'(\gamma) = \max_{i=1,\ldots,N} \frac{1}{M} \sum_{j=1}^{M} I_{w_j \in C_{t_i}}$$

exceeds the threshold P. Under the assumption that all the random extractions are independent, the following theorem characterizes the accuracy of our approximation.
Theorem for the Approximate estimation of $C(\gamma)$
Given ϵ, β, and $\delta \in (0,1)$, $C'(\gamma)$ is an approximate estimate of $C(\gamma)$ to accuracy 2ϵ and level β with confidence $1 - \delta$ in the sense that

$$\mathcal{Q}\{t \in [0\ T] : PC(t) > C'(\gamma) + 2\epsilon\} \leq \beta,$$

with probability greater than $1 - \delta$.

Notice that the number of samples needed to achieve a certain approximation level is independent of the nature of the sample space and of the probability distribution. In particular, the computational load does not significantly increase in the 3D case with respect to the 2D case. This is not the case if one resorts to numerical methods based on gridding or to approximate analytic methods such the one in [16].

2.4 Validation and Tuning

The performance of the conflict detection scheme was evaluated using a three step process:

1. Given the flight plans of two aircraft, generate trajectories and radar measurements over a 20 minutes horizon using the discretized version of the validation model.

ϕ	d_{min}	t_{min}		
		8	12	20
30	0	(N.D.)/1.0	(N.D.)/1.0	(N.D.)/1.0
30	5	0.35/0.80	0.20/0.71	0.19/0.75
30	10	0.17/0.64	0.17/0.68	0.17/0.84
45	0	(N.D.)/1.0	(N.D.)/1.0	0.26/0.80
45	5	0.19/0.75	0.22/.80	0.20/0.78
45	10	0.41/0.60	0.16/0.77	0.11/0.76
90	0	(N.D.)/1.0	(N.D.)/1.0	0.26/0.80
90	5	0.27/0.78	0.13/0.83	0.21/0.84
90	10	0.01/1.0	0.21/0.80	0.17/0.93

Table 2.1: P(FA)/P(SA) for our algorithm.

2. For every value of the - discretized - threshold:

   (a) Execute the detection algorithm at every radar measurement time.

   (b) Compute the *probability of false alarm* P(FA) (fraction of declared conflicts that did not materialize) and the *probability of successful alert* P(SA) (fraction of conflicts declared at least 60 seconds before they occur).

3. Plot the *System Operating Characteristic* (SOC) curve and choose the optimal threshold P.

The SOC is a plot of P(SA) versus P(FA), parameterized by the threshold. In principle, the more the SOC curve approaches the point $(0, 1)$, the better the performance of the system is likely to be. P is typically chosen to correspond the point on the the SOC curve closest to $(0, 1)$, in an attempt to achieve an "optimal" compromise between P(FA) and P(SA) [13].

To ensure our results are reasonable, we compare the performance of our algorithm with the algorithm of [16], which is based on the same description of the uncertainty. The measure of criticality used by [16] is the probability of conflict at the point of the minimum nominal separation. An estimate for this quantity is computed for the 2D case by an analytical over-approximation of the integral of the probability density function for the separation. To compare the two algorithms we also restrict our algorithms to the 2D case, and to simple crossing encounters, parameterized by the path crossing angle ϕ (deg), the minimum nominal separation d_{min} (nmi), and the nominal time t_{min} (min) to d_{min}. The speeds of the aircraft are kept fixed ($v_1 = 480$ nmi/h and $v_2 = 500$ nmi/h). Tables 2.1 and 2.2 summarize the values of P(FA) and P(SA) corresponding to the optimal threshold for different encounter situations computed by running the two detection algorithms ($\epsilon = 0.05$, $\delta = 0.1$, $\beta = 0.05$). Note that when the minimum nominal distance is 0 nmi, in some entries of Table 2.1 and 2.2 P(SA)=1, whereas the optimal P(FA) is not defined. The reason is that for $d_{min} = 0$ nmi there is almost always a conflict, therefore, the optimal threshold is determined by maximizing P(SA), and there are not enough samples to get a statistically significant estimate of P(FA).

Both algorithms give a similar value for P(SA), but P(FA) is lower with our algorithm. The reason for this is that the measure of criticality used in [16] is an over approximation of

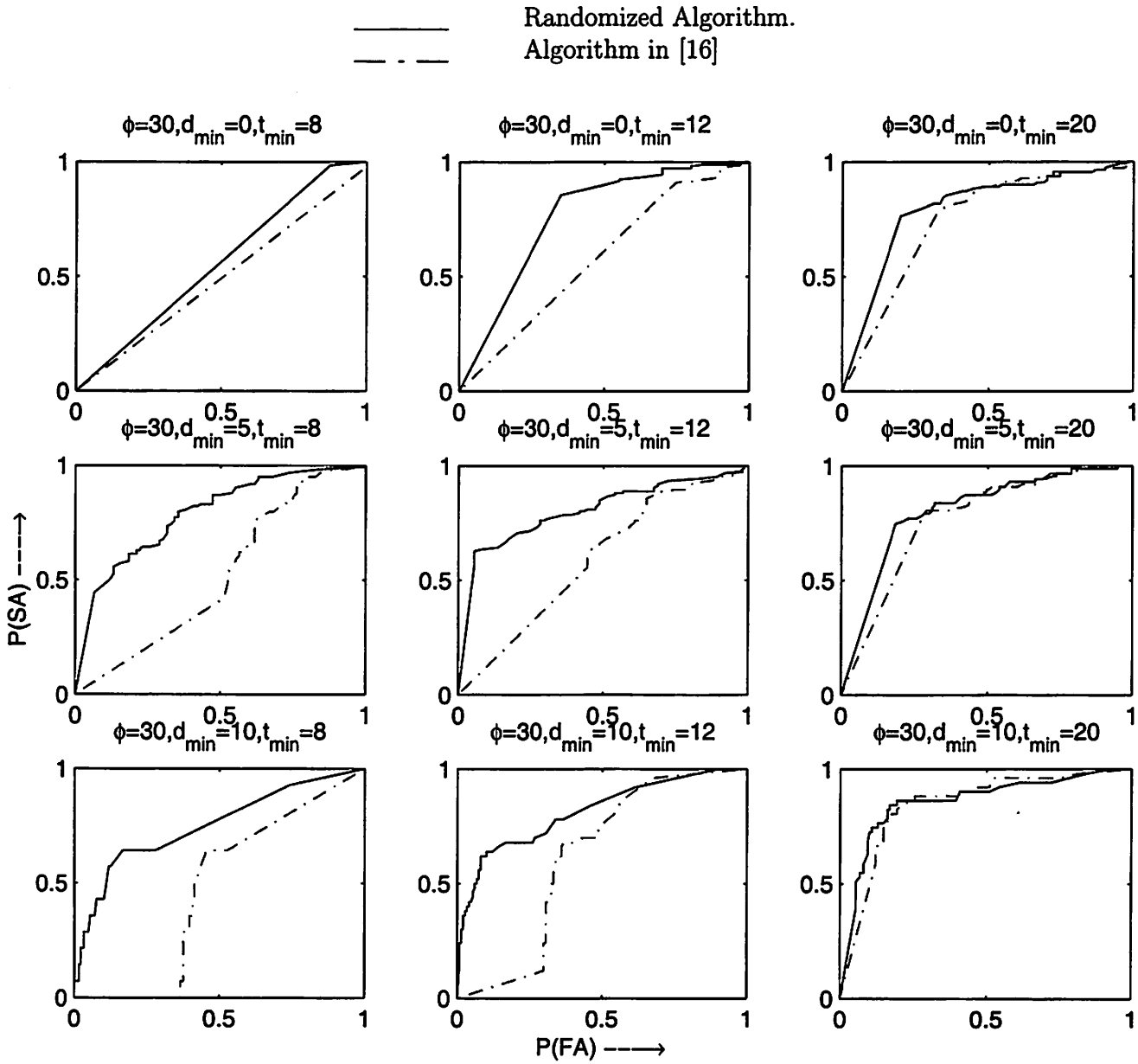

Figure 2.3: System Operating Curves ($\phi = 30°$) for the randomized algorithm and the algorithm in [16]

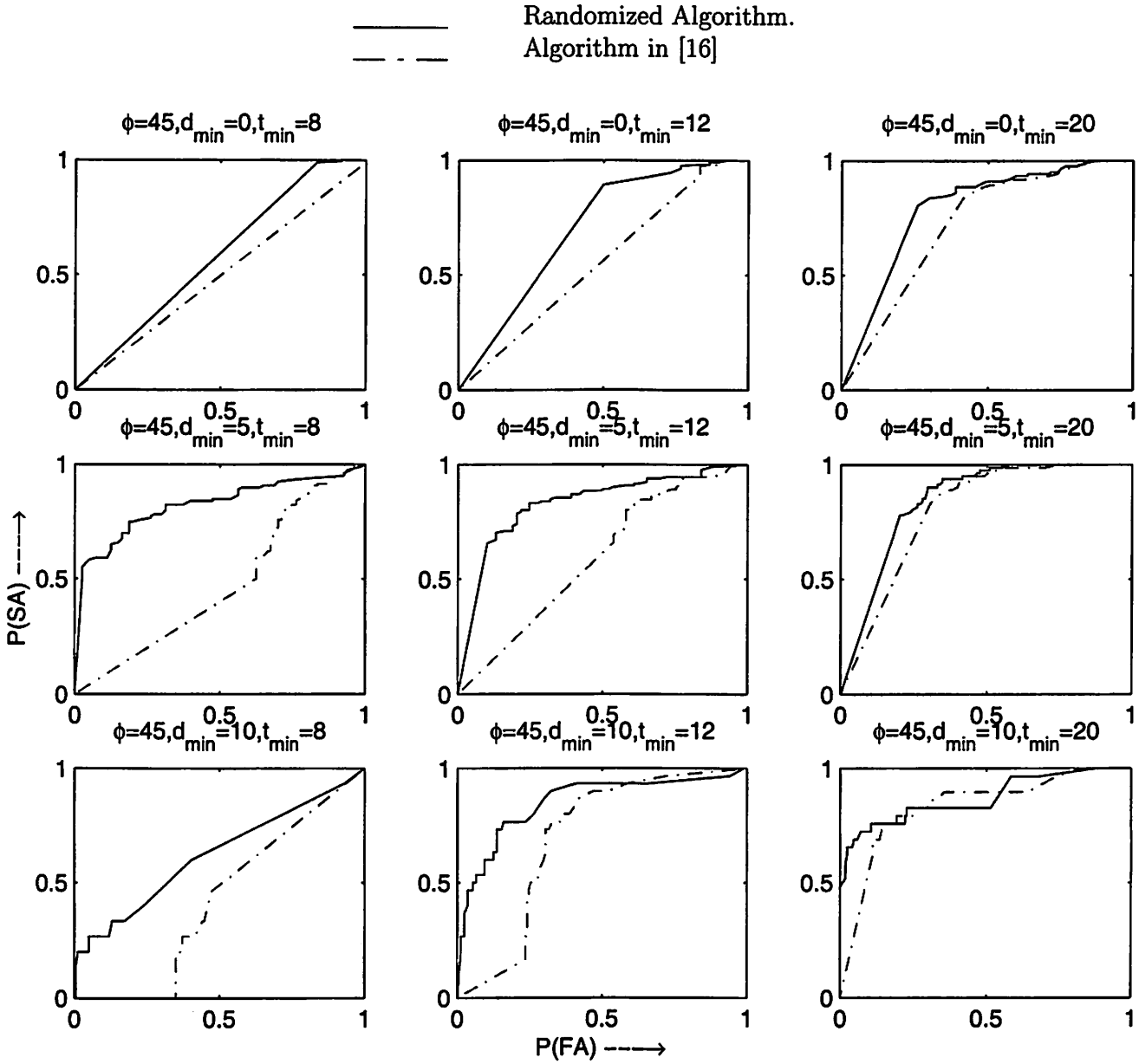

Figure 2.4: System Operating Curves ($\phi = 45°$) for the randomized algorithm and the algorithm in [16]

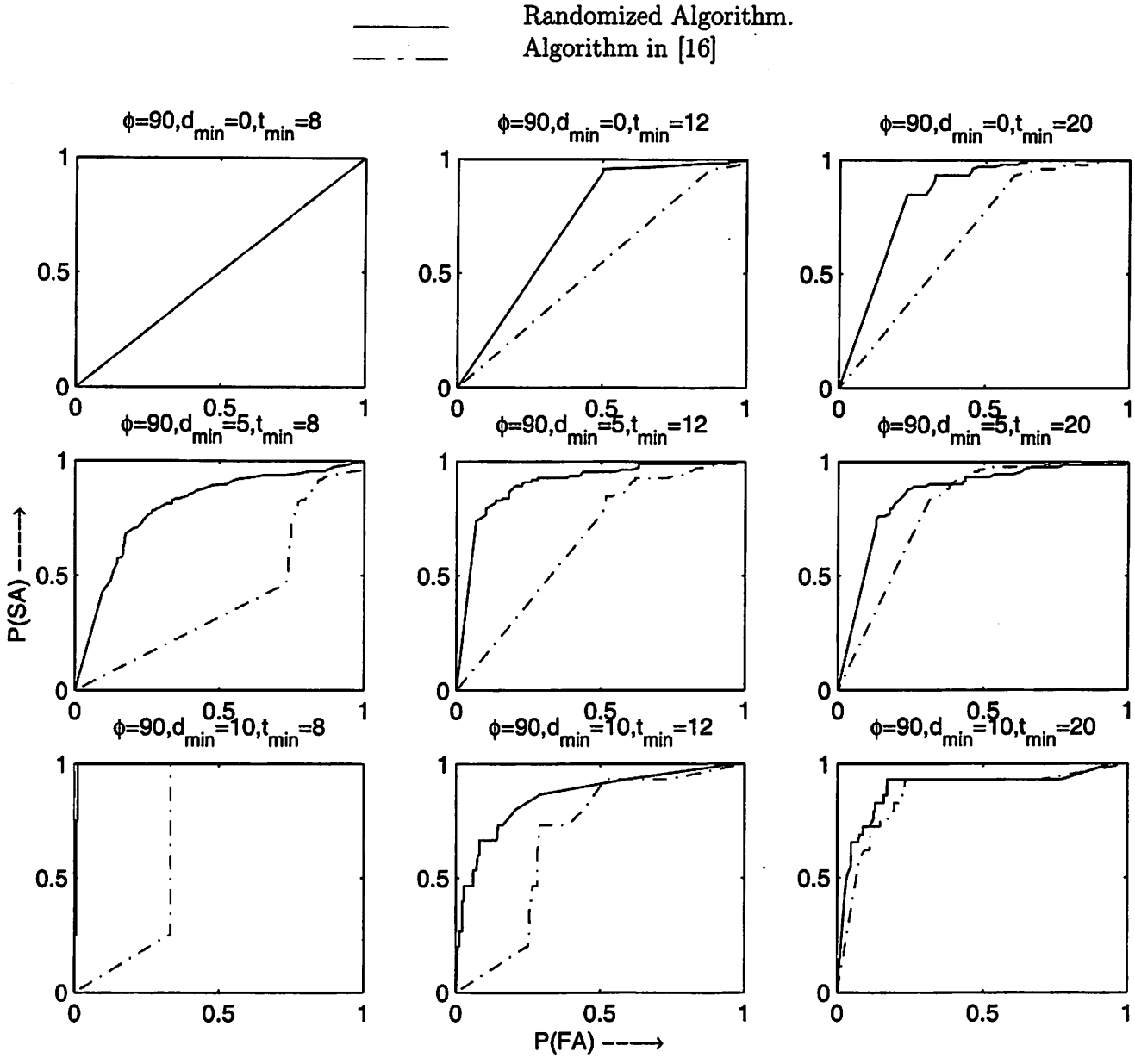

Figure 2.5: System Operating Curves ($\phi = 90°$) for the randomized algorithm and the algorithm in [16]

ϕ	d_{min}	t_{min}		
		8	12	20
30	0	(N.D.)/1.0	(N.D.)/1.0	(N.D)/1.0
30	5	0.61/0.76	0.46/0.63	0.28/0.79
30	10	0.45/0.64	0.37/0.68	0.21/0.84
45	0	(N.D.)/1.0	(N.D.)/1.0	0.43/0.84
45	5	0.70/0.76	0.58/0.80	0.31/0.83
45	10	0.48/0.47	0.33/0.77	0.14/0.76
90	0	(N.D.)/1.0	(N.D.)/1.0	0.42/0.84
90	5	0.76/0.79	0.52/0.85	0.31/0.84
90	10	0.33/1.0	0.30/0.73	0.23/0.93

Table 2.2: P(FA)/P(SA) for the algorithm of [16].

ϕ	d_{min}	t_{min}		
		8	12	20
30	5	0.24/0.64	0.30/0.76	0.31/.82
45	5	0.19/0.75	0.22/0.80	0.22/0.80
90	5	0.21/0.71	0.21/0.90	0.28/0.89

Table 2.3: P(FA)/P(SA) with P=0.85 for our algorithm.

the probability of conflict at t_{min}.

Different configurations lead to different SOC curves and therefore to different optimal thresholds. In [16] the threshold is set using heuristic arguments. We choose the threshold based on the optimal thresholds corresponding to Table 2.1 for the case of $d_{min} = 5$ *nmi*. This typically turns out to be the most interesting case, since the cases $d_{min} = 0$ *nmi* and $d_{min} = 10$ *nmi* correspond to extreme situations in which either a conflict almost always occurs or there is a negligible number of conflicts, respectively. Setting $P = 0.85$ leads to the values of P(FA) and P(SA) reported in Table 2.3.

A sensitivity analysis of the dependence of P on the flight plans to allow us to choose appropriate values for P for the typically encountered configurations. Other aspects that should be taken into account in this process are the detection of conflict a certain amount of time before it occurs and the prediction of its occurrence time. These aspects highly influence the effectiveness of a prediction/resolution scheme involving the human-in-the-loop component.

Chapter 3

2-D conflict resolution of multiple aircraft using convex optimization techniques

3.1 Introduction

In chapter 2, we developed a conflict detection tool. The obvious next step is to design a conflict resolution tool. In this chapter, we study the conflict resolution problem of multiple aircraft in the two dimensional case. In the TRACON area, it is not rare to encounter these kinds of situations. Multiple aircraft conflict resolution is combinatorial in nature. As in [10], our approach is to solve the multiple aircraft conflict resolution using convex optimization algorithms. A cost function is defined which is suitably selected so as to take into account various practical factors such as passenger comfort, fuel efficiency, etc... In [3] [6], convex optimization techniques are used where the resolution maneuvers are parameterized by means of a finite number of variables. Formulating the problem as a finite dimensional optimization problem has inherent advantages: (a) It makes the problem more tractable (b) it allows pilots and the air traffic controllers to exchange trajectory specifications in a simple way. The resultant optimization problems are non convex, but we can have an efficient convex relaxation which gives a near optimal solution. If we add some practical constraints such as velocity constraints or the turning angle (way point constraints), the optimization problem will have a non-linear constraint set. Adding velocity constraints means restricting the speed change of the aircraft. This is important due to following reasons;

1. An aircraft needs to have a minimum velocity to maintain a minimum lift force to fly . If it flies less than that velocity, it will lose its stability.

2. Different aircraft have different engine capacities which will limits the maximum achievable velocity of the aircraft. .Due to the statement (1) and (2), the velocities of each aircraft are limited to a certain range.

3. Pilots and controller don't prefer to use velocity change as a control.

The turning angle constraints have practical implications.The turning angle of the aircraft cannot be too abrupt. This is very important in the passenger's comfort point of view.

Moreover, the physics of the aircraft restricts the implementation of a flight plan which consist of a very large turning angle. The induced nonlinearity due to the inclusion of these constraints are efficiently handled with the use of SOCP.

The chapter is organized in the following manner. In section 2, we describe convex optimization techniques with an emphasis to the quadratic programming and the second order cone programming. In section 3.3, the notion of energy of maneuvers is proposed. The problem is to select from among all conflict free maneuvers the "optimal" ones, where two or more aircraft are in conflict. We also study the maneuvers with minimum energy. Resolution maneuvers are also classified to obtain different types of constraints. We apply convex relaxation and the problem is formulated as a standard convex optimization form. In section 3.4, we present our simulation result.

3.2 Convex Optimization

3.2.1 Basic definitions and properties

Important definitions and properties are described in this section [2].

3.2.2 Definitions

A function $f : R^n \rightarrow R$ is convex if $\mathbf{dom} f$ is a convex set and if for all $x, y \in \mathbf{dom} f$, and θ with $0 \leq \theta \leq 1$, we have,

$$f(\theta x + (1-\theta)y) \leq \theta f(x) + (1-\theta) f(y) \tag{3.1}$$

Geometrically, this inequality means that the line segment between $(x, f(x))$ and $(y, f(y))$ (the chord from x to y) lies above the graph.

A function f is strictly convex if strict inequality holds in (3.1) whenever $x \neq y$ and $0 < \theta < 1$.

A function f is concave if $-f$ is convex, and strictly concave if $-f$ is strictly convex.

A function f is affine if we always have a equality in (3.1). So all affine and linear functions are both convex and concave.

Figure 3.1: Graph of a convex function, where the chord between two points lies above the graph

3.2.3 First Order Condition

If f is differentiable (i,e, it's gradient ∇f exists at each point in **dom**f, which is open), then f is convex if and only if

$$f(y) \geq f(x) + \nabla f(x)^T(y - x) \tag{3.2}$$

hold for all $x, y \in$ **dom**f.This inequality is illustrated below,

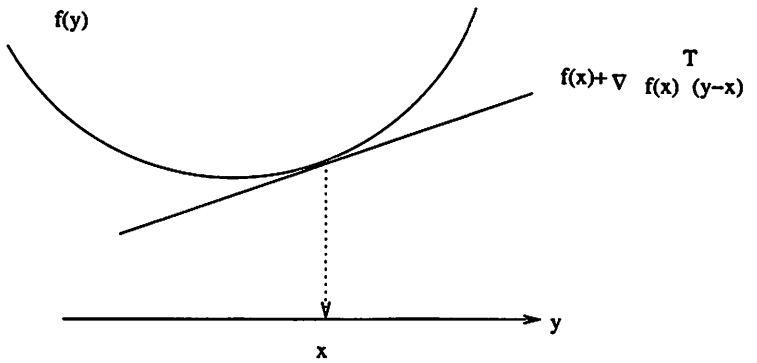

Figure 3.2: if f is a convex function,$f(y) \geq f(x) + \nabla f(x)^T(y - x)$

The above inequality states that for a convex function, the first order Taylor approximation is in fact global under-estimator of the function. Conversely, if the first order Taylor approximation of a function is always a global under-estimator of the function, then the function is convex. This shows that from local information about a convex function (i.e. it's derivative at a point), we can derive global information. This very important property of convex function helps getting efficient solution in convex optimization problems.

3.2.4 Second Order Condition

If f is twice differentiable, i.e., its Hessian or second derivative $\nabla^2 f$ exits at each point in **dom**f, which is open. The f is convex if and only if its Hessian is positive semidefinite
$\nabla^2 f(x) \succeq 0$

for all $x \in$ **dom**f. For a function on R, this reduces to the simple condition$f'' \geq 0$.

3.2.5 Optimization

The basic optimization problem can be formulated as,
minimize $f_0(x)$
subject to $f_i(x) \leq 0, i = 1, ..., m$
$h_i(x) = 0, i = 1, ...p$

This problem is to find an x that minimizes $f_o(x)$ among all x such satisfy the conditions $f_i(x) \leq 0, i = 1, ...m$ and $h_i(x) = 0, i = 1, ...p$. $x \in R^n$ is the optimization variable and the function $f_0 : R^n \rightarrow R$ the objective function or the cost function. The inequalities $f_i(x) \leq 0$ are called inequality constraints and the $h_i(x) = 0$ are the equality constraints.If there is no constraint, the problem is said to be unconstrained.

The problem above is a convex optimization problem if $f_0, f_1, f_2, ..., f_m$ are convex functions and $h_i(x) = a_i^T x - b_i$. The additional requirements for a standard optimization problem to be a convex optimization problem are:

1. The objective is convex.
2. The inequality constraint functions are convex.
3. The equality constraint functions $h_i(x) = a_i^T x - b_i$ are affine.

3.2.6 Quadratic Optimization Problem

The convex optimization problem in the section 3.2.5 is called a quadratic problem (QP) if the objective function is convex and quadratic, and the constraints functions are affine. A quadratic program can be expressed in the form,
minimize $x^T P x + 2q^T x + r$
subject to $Gx \preceq h$
$Ax = b$
where $P = P^T \succ 0$. In a quadratic program, we minimize a convex quadratic function over a polyhedron.

3.2.7 Second-order cone Optimization Problem

A second order cone program (SOCP) can be expressed in the following way,
minimize $c^T x$
subject to $\|A_i x + b_i\| \leq c_i^T x + d_i, i = 1, 2, ..., N$
$Fx = g$
Where $x \in R^n$ is the optimization variable and the norm appearing in the constraints is the Euclidean norm. The constraint $\|A_i x + b_i\| \leq c_i^T x + d_i$ is a second-order cone constraint, since it is the same as requiring the affine function $(Ax + b, c^T x + d)$ to lie in the second-order cone in R^{k+1}.

If $c_i = 0$, the above SOCP is equivalent to quadratic constraint Quadratic programming problem. That means, a problem with a quadratic objective function and the quadratic constraints can be solved in this framework. SOCP is more general and can also take the form LP (Linear Programming), where we have to put the value of A_i, b_i as zero.

3.3 Optimal two legged Maneuver for the multiple aircraft Resolution

3.3.1 Classification of Resolution Maneuvers

The classification of different types of maneuvers can be done by the method described in [9]. Two resolution maneuvers can be classified as qualitatively identical - or of the same "type" -, if there exists a continuous conflict-free deformation of one to the other. Distinguishing between maneuvers based on their "type" is useful, since if the aircraft involved in an encounter situation negotiate a certain resolution type at an early stage, it is preferable that they stick to the chosen type throughout the whole encounter. As, in [9], we know that each resolution maneuver has a natural representation as a braid, and that the classification of maneuvers in homotopy types can be reformulated as the classification of braids in isotope classes, which is a well-studied problem in mathematics. This will lead to the complete characterization of homotopy types of resolution maneuvers given in [9]. If we consider n aircraft (numbered from 1 to n) flying at the same altitude, where each aircraft, say i, flies from position $a_i \in R^2$, at time t_0, to position $b_i \in R^2$, at time t_f. Denote with P_i the space of all continuous maneuvers in R^2 which start from a_i at time t_0 and end at b_i at time t_f, *i.e.*,

$$P_i = \{\alpha_i \in C(T_h, R^2) : \alpha_i(t_0) = a_i, \alpha_i(t_f) = b_i\}, \quad i = 1, \cdots, n,$$

where $C(T_h, R^2)$ denotes the set of all continuous maps from $T_h = [t_0, t_f]$ to R^2. Define $P = \prod_{i=1}^{n} P_i$. Each element $\alpha = (\alpha_1, \cdots, \alpha_n) \in P$ is called a (joint) maneuver for the n aircraft encounter, or an n-maneuver if we want to emphasize the number of aircraft involved. The *minimum separation over encounter (MSE)* for an n-maneuver α is defined to be the minimum distance between any aircraft pair during the whole interval T_h, *i.e.*,

$$\Delta(\alpha) = \min_{1 \le i < j \le n} \inf_{t \in T_h} \|\alpha_i(t) - \alpha_j(t)\|.$$

The set of conflict-free maneuvers is then given by

$$P(R) = P \setminus \Delta^{-1}([0, R]) = \{\alpha \in P : \Delta(\alpha) > R\},$$

where R is the prescribed safe distance assigned to be 5 nmi in en-route airspace. We distinguish different classes of maneuvers in $P(R)$ according to the method of equivalence relation given in [9].

3.3.2 Cost Function

We consider n aircraft flying at the same altitude, with starting positions $a_i \in R^2$, $i = 1, \cdots, n$, at time t_0 and destination positions $b_i \in R^2$, $i = 1, \cdots, n$, at time t_f. The set of maneuvers for aircraft i, P_i, is defined to be the set of all continuous, well defined paths in R^2 which start from a_i at time t_0 and end at b_i at time t_f. The set of n-maneuvers P and the minimal separation over encounter $\Delta(\alpha)$, $\alpha \in P$, are defined similarly as in the previous section 3.3.1, whereas $P(R)$ is defined to be the set of all n-maneuvers with a MSE greater than *or equal to* R. This modification is in order to ensure that $P(R)$ is a closed set, so that

for the optimization problems we encounter later, the optimal value is in fact attained by some maneuver in $P(R)$.

We propose the *energy* of an n-maneuver as cost function to be optimized. Consider the maneuver of a single aircraft, say $\alpha_i \in P_i$. The energy of α_i is defined as

$$J(\alpha_i) = \int_{t_0}^{t_f} ||\dot{\alpha}_i(t)||^2 \, dt, \quad i = 1, \cdots, n. \tag{3.3}$$

Then, the *energy* of an n-maneuver $\alpha = (\alpha_1, \ldots, \alpha_n) \in P$ is simply the sum of the energies of all α_i, $i = 1, \cdots, n$, *i.e.*,

$$J(\alpha) = \sum_{i=1}^{n} J(\alpha_i). \tag{3.4}$$

The application of Cauchy-Schwartz inequality to equation (4.1) yields

$$J(\alpha_i) \geq [L(\alpha_i)]^2/(t_f - t_0),$$

where the equality holds if and only if $\|\dot{\alpha}_i(t)\|$ is constant, *i.e.*, if and only if the motion of aircraft i is of constant speed $L(\alpha_i)/(t_f - t_0)$. This serves our purpose perfectly since, if one ignores the presence of other aircraft, the J-minimal maneuver for aircraft i is the constant speed motion along the line segment joining a_i to b_i. If the maneuver is required to lie on some curve other than the line segment, then of all the different parameterizations, the one with the least energy is the one with constant speed. This has a practical counterpart in our context, since safety, performance limits and passenger comfort prohibit the aircraft from making abrupt turns and speed changes.

Finally, we can formulate the constrained optimization problem we shall deal with as follows:

$$\text{Minimize } J(\alpha) \text{ subject to } \alpha \in P(R). \tag{3.5}$$

The necessary Conditions for Optimal Maneuver r$\alpha^* = (\alpha_1^*, \cdots, \alpha_n^*) \in P(R)$ to be a solution to problem (3.5) is described in [9].

3.3.3 Optimal 2-legged Maneuver for Two Aircraft Conflict Resolution

Consider two aircraft with starting positions $a = (a_1, a_2)$ and destination positions $b = (b_1, b_2)$. Let $\alpha = (\alpha_1, \alpha_2)$ be a 2-legged maneuver with way-points $c_{i,j}$, $i = 1, 2$, $j = 0, 1, 2$. Since $c_{i,0} = a_i$ and $c_{i,2} = b_i$ are fixed, the only way-points we can actually choose are $c_{i,1}$, $i = 1, 2$, which we then denote with $c_i = c_{i,1}$ to simplify the notations. Assume that the epoch corresponding to the middle way-points is $t_c \in (t_0, t_f)$. After some calculations, the cost function for α rewritten in terms of c_1 and c_2 can be simplified to

$$J(\alpha) = \frac{t_f - t_0}{(t_f - t_c)(t_c - t_0)}[\|c_1 - c_1^u\|^2 + \|c_2 - c_2^u\|^2] + C, \tag{3.6}$$

where C is a constant, and c_i^u is defined by

$$c_i^u = \frac{(t_f - t_c)a_i + (t_c - t_0)b_i}{t_f - t_0}, \quad i = 1, 2. \tag{3.7}$$

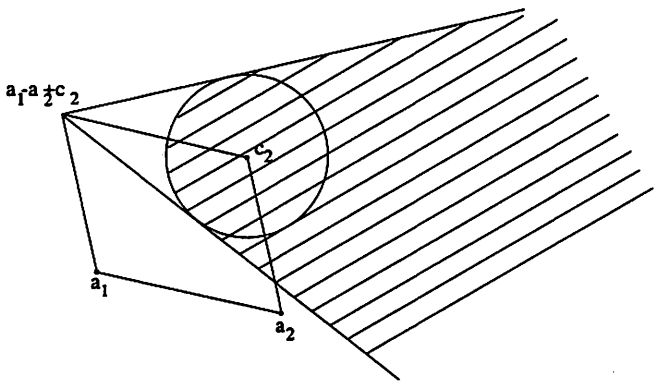

Figure 3.3: Plot of $\{c_1 : d^*(a_1 - a_2, c_1 - c_2) \geq R\}$

Note that c_1^u and c_2^u are the optimal way-points when minimizing $J(\alpha)$ without the MSE constraint. In the braid representation, they correspond to the intersections of the horizontal plane $t = t_c$ with the lines joining (a_1, t_0) to (b_1, t_f) and (a_2, t_0) to (b_2, t_f), respectively.

The MSE constraint can also be simplified. For example in the first stage of the 2-legged maneuver, the motions of the two aircraft are:

$$\alpha_1(t) = a_1 + (c_1 - a_1)\frac{t - t_0}{t_c - t_0}, \quad \alpha_2(t) = a_2 + (c_2 - a_2)\frac{t - t_0}{t_c - t_0}, \quad t_0 \leq t \leq t_c. \tag{3.8}$$

Simple calculations show that

Lemma 3.3.1 *Set* $\lambda = (a_1 - a_2)^T(c_1 - c_2 - a_1 + a_2)$. *Then, the minimum distance of the two aircraft during the time interval* $[t_0, t_c]$ *is*

$$d^* = \begin{cases} \|a_1 - a_2\|, & \text{if } \lambda > 0; \\ \|c_1 - c_2\|, & \text{if } \lambda < -\|c_1 - c_2 - a_1 + a_2\|^2; \\ \sqrt{\|a_1 - a_2\|^2 - \lambda^2/\|c_1 - c_2 - a_1 + a_2\|^2}, & \text{if } -\|c_1 - c_2 - a_1 + a_2\|^2 \leq \lambda \leq 0. \end{cases}$$

By inspection we can see that d^* is a function of relative positions $a_1 - a_2$ and $c_1 - c_2$ only, and it is independent of the time t_c. Hence, we shall use $d^*(a_1 - a_2, c_1 - c_2)$ to denote it explicitly whenever necessary. For the last stage of the maneuver, the motions can be written in a similar way as

$$\alpha_1(t) = c_1 + (b_1 - c_1)\frac{t - t_c}{t_f - t_c}, \quad \alpha_2(t) = c_2 + (b_2 - c_2)\frac{t - t_c}{t_f - t_c}, \quad t_c \leq t \leq t_f. \tag{3.9}$$

Then, the minimum distance between the two aircraft during time interval $[t_c, t_f]$ is $d^*(c_1 - c_2, b_1 - b_2)$ and, hence, the overall MSE is $\Delta(\alpha) = \min\{d^*(a_1 - a_2, c_1 - c_2), d^*(c_1 - c_2, b_1 - b_2)\}$.

To ensure that the maneuver belongs to $P^2(R)$, both $d^*(a_1 - a_2, c_1 - c_2)$ and $d^*(c_1 - c_2, b_1 - b_2)$ have to be at least R. Fix c_2, and suppose we have the freedom of choosing c_1 arbitrarily. Figure 3.3 shows the set $\{c_1 : d^*(a_1 - a_2, c_1 - c_2) \geq R\}$ as a shaded region, which is obtained by drawing a circle of radius R around c_2 and the two lines starting from point $a_1 - a_2 + c_2$ and tangent to that circle. This is always possible since, by the assumption

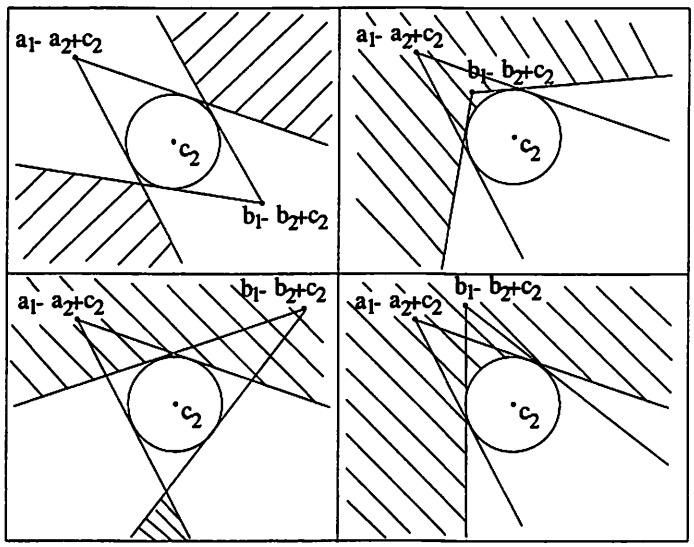

Figure 3.4: The 4 possible configurations of the f easible set for c_1 given a fixed c_2.

$\|a_1 - a_2\| > R$, $a_1 - a_2 + c_2$ is outside of the circle. The set $\{c_1 : d^*(c_1 - c_2, b_1 - b_2) \geq R\}$ can be obtained in a similar way. Then, the final feasible set for c_1 given c_2 is the intersection of these two sets and, depending on the relative position of $a_1 - a_2$ and $b_1 - b_2$, it has four possible configurations which are shown in Figure 3.4. Denote this feasible set as $A(c_2)$ to highlight its dependence on c_2. Notice that $A(c_2)$ has the important property to be invariant with respect to translation: $A(c_2)$ for different c_2 can be obtained simply by translation. In particular, if we consider the set $A(0)$, then for any $c_2 \in R^2$, $A(c_2) = c_2 + A(0)$.

As a result of the above simplifications, optimization problem for a 2-legged maneuver involving two aircraft degenerates into:

$$\text{Minimize } \|c_1 - c_1^u\|^2 + \|c_2 - c_2^u\|^2 \text{ subject to } c_1 \in A(c_2), c_2 \in R^2. \tag{3.10}$$

Problem (3.10) can be considerably simplified if we observe that in all but the first configuration, the unconstrained optimal c_1^u, c_2^u are feasible, and hence they represent the (trivial) optimal way-points for problem (3.10). In fact, notice that by equation (3.7),

$$c_1^u - c_2^u = \frac{t_f - t_c}{t_f - t_0}(a_1 - a_2) + \frac{t_c - t_0}{t_f - t_0}(b_1 - b_2)\,. \tag{3.11}$$

So if we choose $c_2 = c_2^u$ in Figure 3.4, then c_1^u lies on the line segment between $a_1 - a_2 + c_2$ and $b_1 - b_2 + c_2$, and is feasible in the last three configurations.

Therefore we shall now consider only the first configuration or, equivalently, we assume that a and b are chosen such that there is a conflict for the unconstrained optimal maneuver, *i.e.*, the constant velocity motions connecting a_i to b_i for $i = 1, 2$. Then, for any fixed c_2, the feasible set $A(c_2)$ of c_1 is the union of two disjoint convex sets corresponding to the two fundamental types of maneuvers. Let

$$q = \frac{t_f - t_c}{t_f - t_0}(a_1 - a_2 + c_2) + \frac{t_c - t_0}{t_f - t_0}(b_1 - b_2 + c_2) \tag{3.12}$$

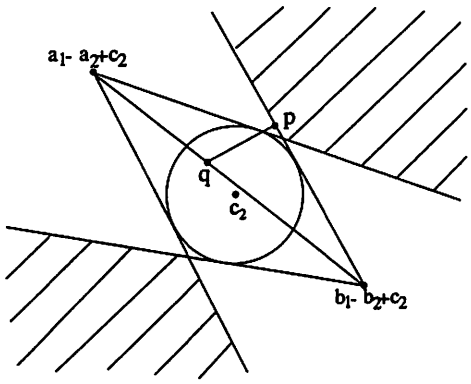

Figure 3.5: Construction of the optimal c_1 and c_2 for the first configuration.

and let p be the point in $A(c_2)$ nearest to q. . If p is not unique, we can choose any of them. This is the case if and only if there is an exact collision for the unconstrained optimal maneuver. In the case when we restrict the feasible set to a single connected component (optimization over a certain type of maneuver), such a p is uniquely defined.

3.3.4 Optimal 2-legged maneuver for Multiple Aircraft Conflict Resolution

We now turn to the problem of finding the optimal 2-legged maneuver for n aircraft encounters. Roughly speaking, the nature of the n aircraft conflict resolution problem is mainly combinatorial in that the major task is to choose the type of resolution maneuver where one can then find the optimal maneuver. There are various heuristics for choosing a resolution type. We shall suggest a randomized type chooser based on a probabilistic resolution algorithm as in [10]. In this subsection, however, we deal with the less difficult task of finding the optimal maneuver within a given type.

Fix $t_c \in T_h$. Suppose we have decided which type of resolution maneuver to use. Then, the problem is to find the way-points $c_1, \cdots, c_n$ which

$$\text{Minimize} \sum_{i=1}^{n} \|c_i - c_i^u\|^2 \text{ subject to } c_i \in A_{ij}^{\pm}(c_j), \quad 1 \le i < j \le n, \tag{3.13}$$

where c_i^u is defined as in (3.7) for $i = 1, \cdots, n$, and $A_{ij}^{\pm}(c_j)$ denote the connected component of the set $A_{ij}(c_j)$ matching our desired resolution type. Here, $A_{ij}(c_j)$ is the feasible set for c_i given c_j and it can be computed as in Section 3.3.3, with a_i, b_i, a_j, b_j in place of a_1, b_1, a_2, b_2. Figure 3.6 represents the four possible configurations of $A_{ij}(c_j)$ depending on the relative position of a_i, b_i, a_j, b_j. Notice that in all but the first configuration, one of the connected component of $A_{ij}(c_j)$ is nonconvex. In general, solving nonconvex programming problems is a great challenge, even when the object function is quadratic. This is the reason why we "linearize" the feasible set by using a half plane inner approximation $A'_{ij}(c_j)$ of $A_{ij}(c_j)$ as shown in Figure 3.6. Although this inner approximation excludes some feasible c_i, it contains the unconstrained optimal c_i^u if c_j is chosen to be c_j^u. Therefore it is expected that the approximation will not be too loose. In the special case when any pair of aircraft is in

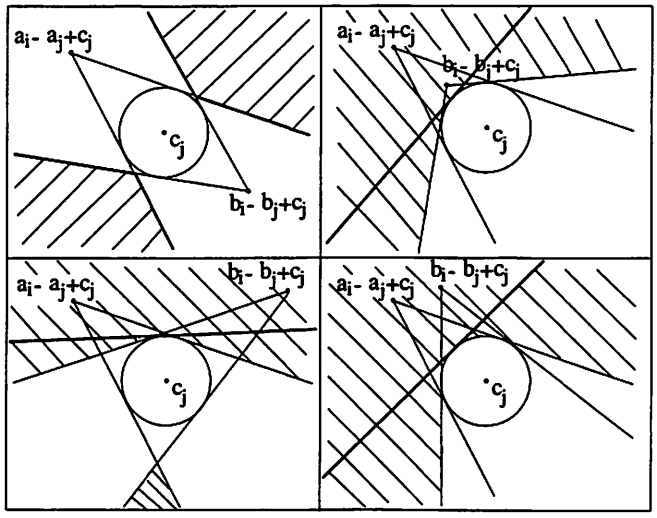

Figure 3.6: Convex approximation of the feasible set for c_1 given c_2.

the first configuration, *i.e.*, the unconstraint optimal joint maneuver would cause a conflict between any aircraft pair, the approximation is tight. A symmetric encounter is such a case, and such encounters are in fact among the most dangerous ones of all possible encounters.

We then have a linearly constrained quadratic optimization problem which can be solved very efficiently by many software packages. For multiple aircraft, we can run the optimization algorithm for each fundamental type and choose the one with the lowest cost.

3.3.5 Velocity Constraints

Each aircraft has a speed limit (the maximum speed with which it can fly) that results from the capability of it's engine. In addition, every aircraft must fly more than a certain velocity to maintain a minimum lift force to keep it in the air. If aircraft fly at excessively high speeds, it becomes very difficult for the Air Traffic controller to handle the traffic efficiently. Moreover, pilots don't prefer a large speed variation during to the course of their flight. As our solution might end up suggesting velocities which can not be implemented in the actual ATC system, it is imperative to add velocity constraints in the optimization process. The constraint should make sure that our algorithm should suggest velocities which will lie within a certain range. The range of velocities can be obtained by accumulating information from the aircraft engine data, pilots and the Air Traffic controllers.

Consider an aircraft with the starting position $\mathbf{a}_i$ and the destination position $\mathbf{b}_i$, where $\mathbf{a}_i, \mathbf{b}i \in R^2$. Let's consider a 2-legged maneuver in $P^2(R)$ with its mid-way-point $\mathbf{c}_i \in R^2$. As it is assumed before, the epoch corresponding to the middle way point is $t_{ci} \in (t_0, t_f)$. We can fix t_c for all the aircraft as t_c^*. Again for 2 legged maneuver, , $t_c^* = 0.5(t_0 + t_f)$. Let V_{max} is the maximum velocity corresponding to the aircraft i. In the time interval $[t_0, t_c^*]$, the aircraft i can be in a circle with a center at a_i and the radius of $V_{max}t_c^*$. Also, in the time interval $[t_c^*, t_f]$, the aircraft i can be in a circle with a center at $\mathbf{b}_i$ and the radius of $V_{max}t_c^*$ The following figure depicts the situation,

The constrains can be mathematically expressed as, where $i = 1, 2..., N$

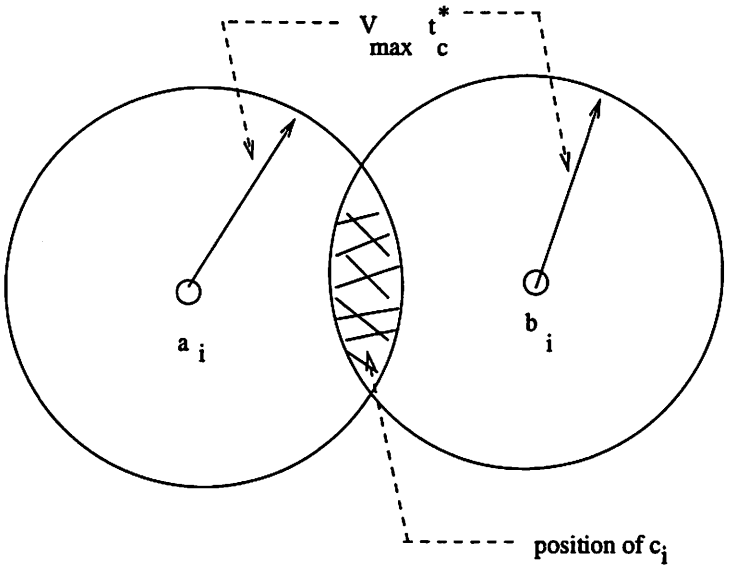

Figure 3.7: Velocity constraints

$\|\mathbf{c}_i - \mathbf{a}_i\| \leq t_c^* V_{max}$
$\|\mathbf{c}_i - \mathbf{b}_i\| \leq t_c^* V_{max}$
which are second-order cone constraints,
For all $i = 1, 2, ..., N$,
$\|\mathbf{c}_i - \mathbf{a}_i\| \leq t_c^* V_{max} + \chi_{ai}^T \mathbf{c}_i$ where $\chi_{ai} = 0$ for all $i = 1, 2, ...N$.
$\|\mathbf{c}_i - \mathbf{b}_i\| \leq t_c^* V_{max} + \chi_{bi}^T \mathbf{c}_i$ where $\chi_{bi} = 0$ for all $i = 1, 2, ..., N$.

We will add $2N$ more second-order cone constraints in the optimization problem

3.3.6 Turning Angle Constraints

The angle each aircraft turns at its way point cannot exceed a certain threshold angle. The turning angle constraints have practical implications.The turning angle of the aircraft cannot be too abrupt from the passengers comfort point of view. Moreover, the physics of the aircraft restricts the implementation of a flight plan which consist of a very large turning angle. So our solution should provide a turning angle which can be implemented in the actual flight plan.

Consider an aircraft with the starting position $\mathbf{a}_i$ and the destination position $\mathbf{b}_i$. Let's consider a 2-legged maneuver in $P^2(R)$ with its mid-way-point $\mathbf{c}_i$. Where, $\mathbf{a}_i, \mathbf{b}_i, \mathbf{c}_i \in R^2$. It is assumed, the epoch corresponding to the middle way point is $t_{ci} \in (t_0, t_f)$. We can fix t_c for all the aircraft as t_c^*. At any point of the flight path, the aircraft is not allowed to turn in an angle which is more than the maximum turning angle α. In the 2-legged maneuver, the maximum turn happens at the mid way-point. The position of $\mathbf{c}_i$ should be chosen such that the flight plan does not violate the tuning angle constraints.

The turning angle constraints can be transferred as Second-order cone constraints. In the Figure 3.8, the aircraft i is taking a turn α at the point $\mathbf{c}_i$. $\mathbf{c}_i$ should lie in a circle where

$\mathbf{a}_i$, $\mathbf{b}_i$ and $\mathbf{c}_i$ are 3 points on the perimeter and $\mathbf{c}_i$ is equidistant from $\mathbf{a}_i$ and $\mathbf{b}_i$ in such a way that the angle $\mathbf{a}_i\mathbf{c}_i\mathbf{b}_i$ is $180^0 - \alpha$ or the outer angle is α. If $\mathbf{c}_i$ always lies in the circle, the maximum turning angle of the aircraft can never be more than than α.

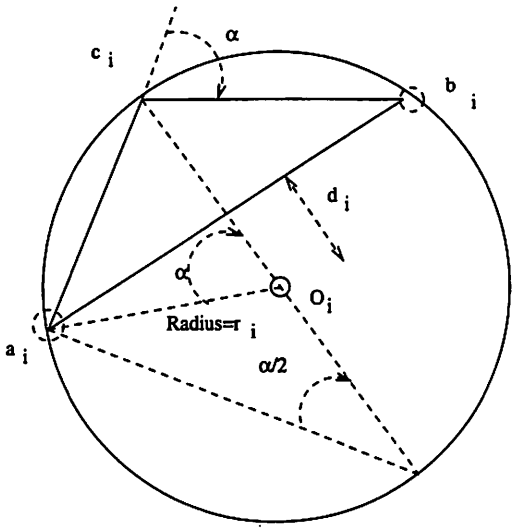

Figure 3.8: Turning angle constraints

The circle with it's center $\mathbf{O}_i \in R^2$ and the radius r_i will define the feasible set for the turning angle constraints for the aircraft i.

Let $d_i \in R$ is the perpendicular distance from the chord $\mathbf{a}_i\mathbf{b}i$ to $\mathbf{O}_i$.

We can get, $d_i = \frac{1}{2}\|\mathbf{b}_i - \mathbf{a}_i\| cot(\alpha)$.

The coordinate of $\mathbf{O}_i$,

$$\mathbf{O}_i = \frac{\mathbf{a}_i + \mathbf{b}_i}{2} + T_{\pm\frac{\pi}{2}} \frac{\mathbf{b}_i - \mathbf{a}_i}{\|\mathbf{b}_i - \mathbf{a}_i\|} d_i \tag{3.14}$$

Where O_i,a_i and b_i are all vectors in R^2.
$T_{\pm\frac{\pi}{2}}$ is the rotation matrix with $\pm\frac{\pi}{2}$ rotation angle.

$$T_{\frac{\pi}{2}} = \begin{pmatrix} 0 & 1 \\ -1 & 0 \end{pmatrix} \tag{3.15}$$

$$T_{-\frac{\pi}{2}} = \begin{pmatrix} 0 & -1 \\ 1 & 0 \end{pmatrix} 0208)(3.16)$$

The radius of the circle r_i,

$$r_i = \frac{\|\mathbf{b}_i - \mathbf{a}_i\|}{2sin(\alpha)} \tag{3.17}$$

The constraints set can be written as equations,

For all $i = 1, 2, .., N$,
$\|\mathbf{c}_i - \mathbf{O}_i\| \leq r_i$

which can also be transfered as a SOCP constraint.
For all $i = 1, 2, .., N$,
$\|\mathbf{c}_i - \mathbf{O}_i\| \leq r_i + \chi_i^T \mathbf{c}_i$
where $\chi_i = 0$ for all $i = 1, 2, .., N$

We get $2N$ such constraints. This optimization problem can be solved using software such as SOCP [15].

3.4 Simulation

Our algorithm is based on a probabilistic model of the aircraft motion which uses the probability of conflict to generate resolution paths. We run the stochastic resolution algorithm first [10]. Then, with a high probability a safe resolution maneuver is generated, but even if this is not the case, the maneuver corresponds to a particular resolution type which can be thought to be a relatively good one. Using this type of resolution, we can then run the convex optimization algorithm to obtain a nearly optimal resolution maneuver within that type. Here, we use the software package SOCP to solve the optimization problem. We ran the algorithm in different scenarios where there are 2,4,8 and 16 aircraft in a potential conflict. We have also varied the conflict zone as $R = 10n.mi.$ and $R = 5n.mi.$. As aircraft are trying to maintain a distance R among themselves while optimizing their flight paths without any coordination among them, our algorithm is a decentralized one. We can see that the deviation from the nominal path is higher for the case $R = 5n.mi$ than the case where $R = 10n.mi.$ We have also used the maximum velocity as 420 n.mi/hour and the maximum turning angle as pi/10. The result of the simulations are presented in Figure 3.9 to Figure 3.16.

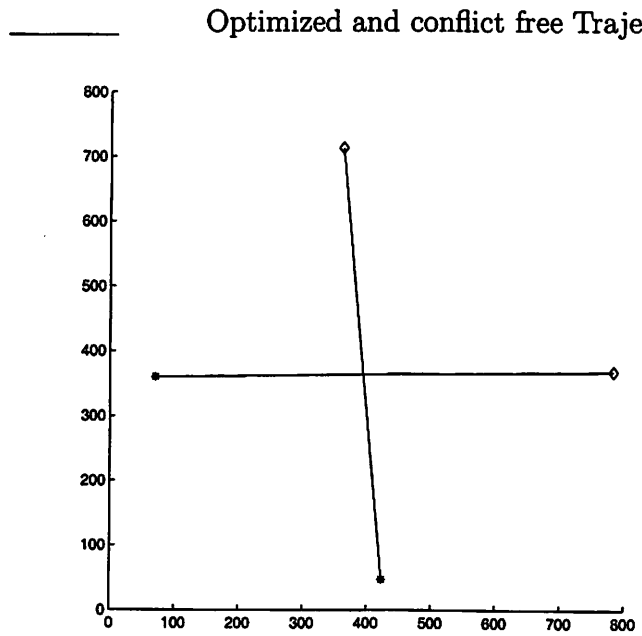

Figure 3.9: Conflict resolution of 2 aircraft with velocity (less than 420.n.mi/hour) and way point constraint (turning angle less than pi/10) and R=5 n.mi

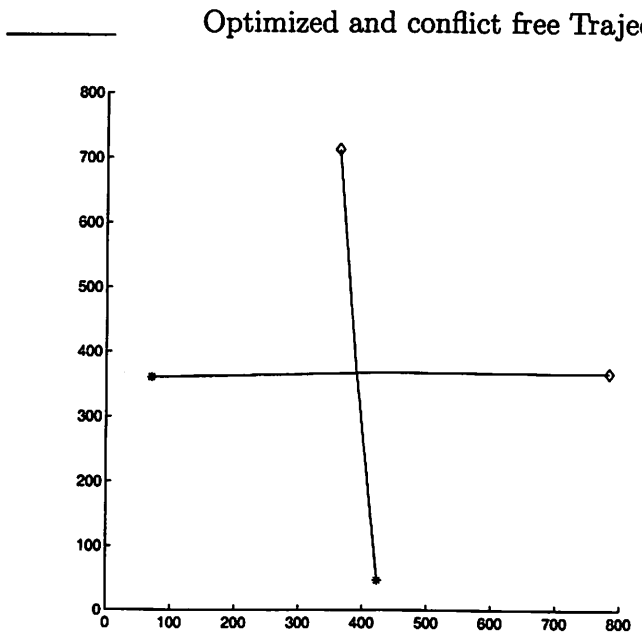

Figure 3.10: Conflict resolution of 2 aircraft with velocity (less than 420.n.mi/hour) and way point constraint (turning angle less than pi/10) and R=10 n.mi

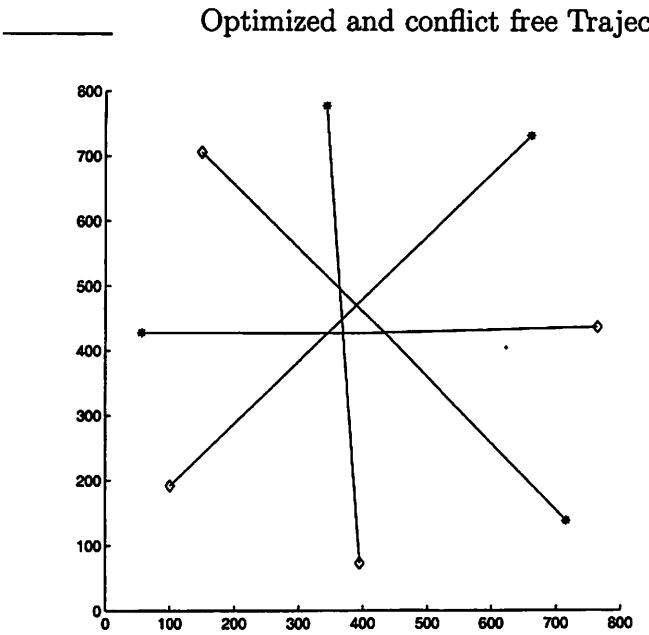

Figure 3.11: Conflict resolution of 4 aircraft with velocity (less than 420.n.mi/hour) and way point constraint (turning angle less than pi/10) and R=5 n.mi

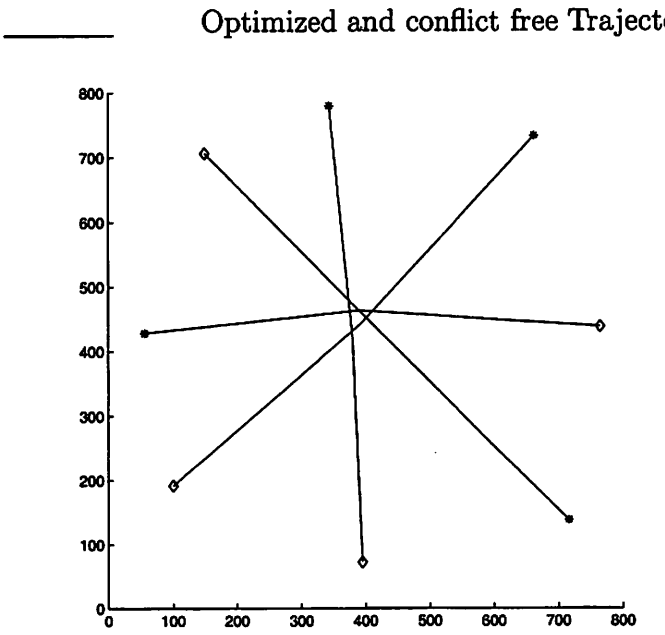

Figure 3.12: Conflict resolution of 4 aircraft with velocity (less than 420.n.mi/hour) and way point constraint (turning angle less than pi/10) and R=10 n.mi

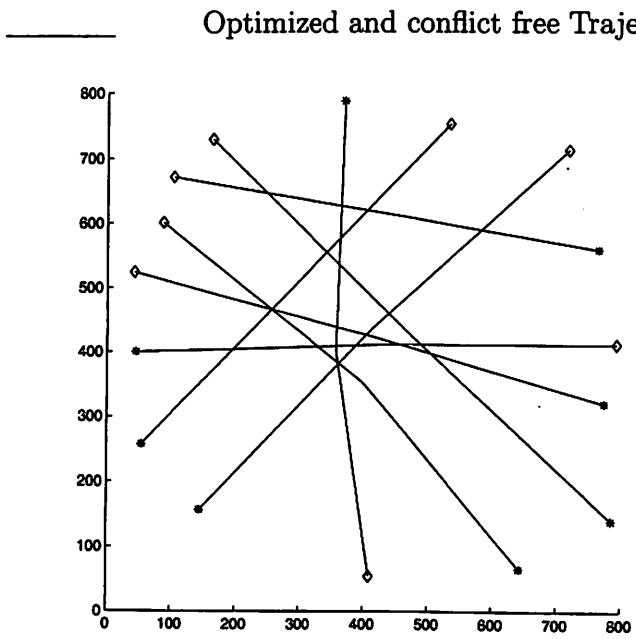

Figure 3.13: Conflict resolution of 8 aircraft with velocity (less than 420.n.mi/hour) and way point constraint (turning angle less than pi/10) and R=5 n.mi

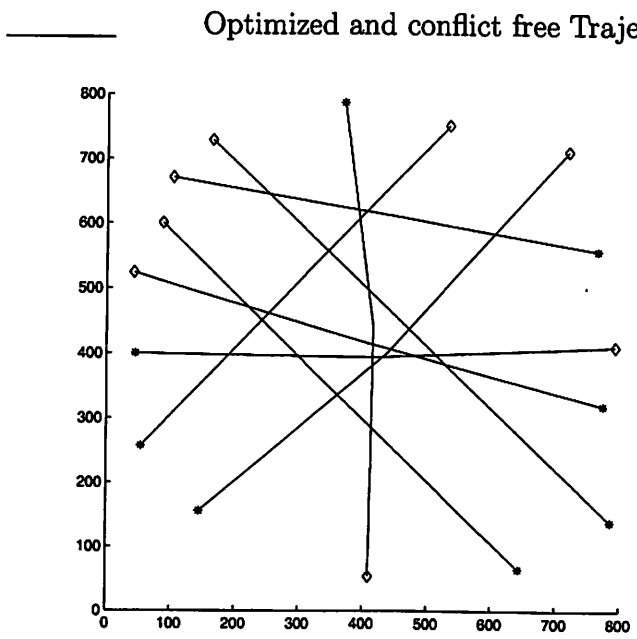

Figure 3.14: Conflict resolution of 8 aircraft with velocity (less than 420.n.mi/hour) and way point constraint (turning angle less than pi/10) and R=10 n.mi

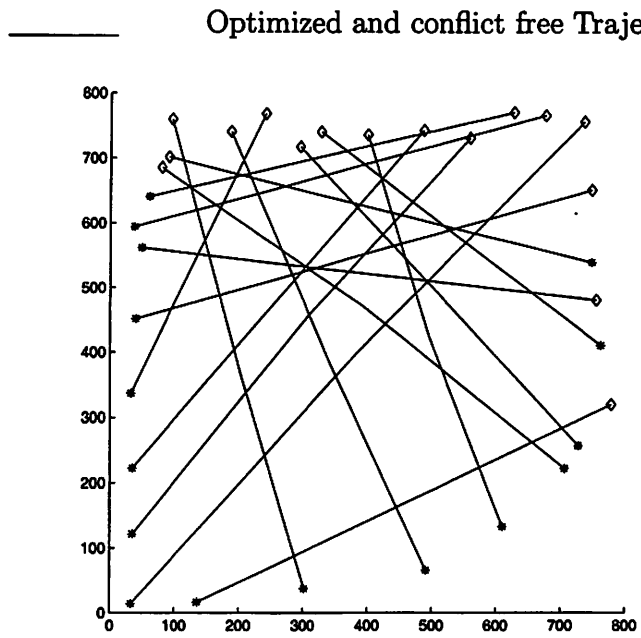

Figure 3.15: Conflict resolution of 16 aircraft with velocity (less than 420.n.mi/hour) and way point constraint (turning angle less than pi/10) and R=5 n.mi

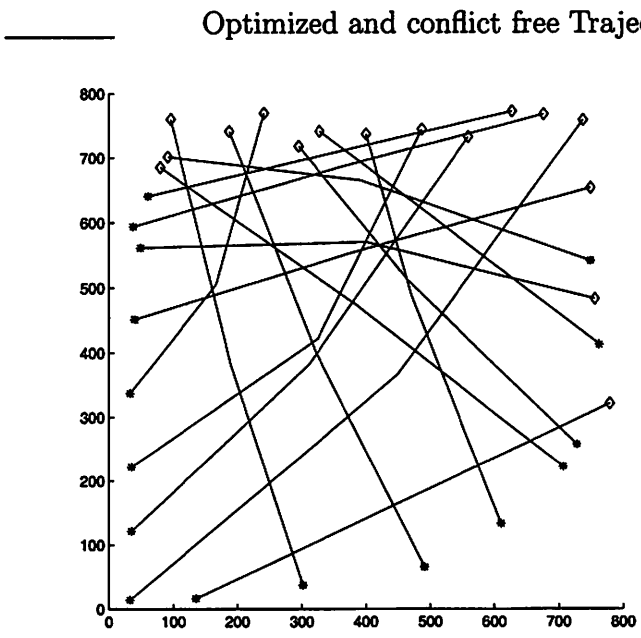

Figure 3.16: Conflict resolution of 16 aircraft with velocity (less than 420.n.mi/hour) and way point constraint (turning angle less than pi/10) and R=10 n.mi

Chapter 4

Three Dimensional Optimal Coordinated Maneuvers for Aircraft Conflict Avoidance

In this chapter, we present the problem of finding optimal three dimensional conflict-free maneuvers for multiple aircraft [7]. The candidate maneuvers include changes of altitude, heading and speed. Among all the conflict-free maneuvers, we try to find the one which minimizes a certain energy function. A priority mechanism is incorporated into the cost function so that aircraft with lower priority assume more responsibility in resolving the conflicts. Moreover, vertical maneuvers are penalized with respect to horizontal ones for the sake of passenger comfort. A geometric construction and a numerical algorithm are given to determine the optimal maneuver in the two aircraft case. As for the multi-aircraft case, an approximation scheme is proposed to compute a suboptimal two-legged solution. Extensive examples are presented to illustrate the effectiveness of the proposed approaches.

4.1 Problem Formulation

Consider a single aircraft, say aircraft i, which flies from position $a_i \in \mathbf{R}^3$ at time t_0 to position $b_i \in \mathbf{R}^3$ at time t_f. Set $T = [t_0, t_f]$, and denote with $\mathbf{P}_i$ the set of all *maneuvers* for aircraft i, i.e., continuous and piecewise C^1 functions $\alpha_i : T \to \mathbf{R}^3$ satisfying $\alpha_i(t_0) = a_i$ and $\alpha_i(t_f) = b_i$

The *energy* of a maneuver $\alpha_i : T \to \mathbf{R}^3$ is defined as

$$J(\alpha_i) = \frac{1}{2} \int_{t_0}^{t_f} ||\dot{\alpha}_i(t)||^2 \, dt, \tag{4.1}$$

which by the Cauchy-Schwartz inequality satisfies

$$J(\alpha_i) \geq \frac{1}{2} \frac{L(\alpha_i)^2}{(t_f - t_0)},$$

where $L(\alpha_i) = \int_{t_0}^{t_f} ||\dot{\alpha}_i(t)|| \, dt$ is the length of the curve α_i. The equality holds if and only if the speed $\|\dot{\alpha}_i(t)\|$ is constant, and in this case the energy $J(\alpha_i)$ is proportional to the

square of the length of α_i. This implies that the maneuver with the least energy for a single aircraft is the constant-speed motion along the line segment from its starting position to its destination position. If the aircraft is forced to move along some fixed curve other than the line segment, then the parameterization of the curve with the least energy is the one with constant speed, and the minimal energy is proportional to the square of the curve length. As a result, the least energy maneuver between two points in the presence of *static* obstacles is the shortest curve between the two points parameterized proportionally to its arc length. This observation will be used later in this chapter , when dealing with the two aircraft case.

In the following development, we assume that a group of aircraft flying in a certain region of airspace have been isolated so that only conflicts among aircraft in this group need to be considered during the time interval of interest. This assumption, although unrealistic, is popular in the current literature on conflict resolution.

Suppose there are n aircraft in the group and they are numbered from 1 to n. Each aircraft, say aircraft i, starts from position $a_i \in \mathbf{R}^3$ at time t_0 and arrives at position $b_i \in \mathbf{R}^3$ at time t_f, $i = 1, \ldots, n$. $\mathbf{P}_i$ is defined as above. Define $\mathbf{P}(\mathbf{a}, \mathbf{b}) = \prod_{i=1}^{n} \mathbf{P}_i$, where $\mathbf{a} = (a_1, \ldots, a_n)$ and $\mathbf{b} = (b_1, \ldots, b_n)$ denote the starting and destination positions of the n-aircraft system respectively. Each element $\alpha = (\alpha_1, \ldots, \alpha_n)$ of $\mathbf{P}(\mathbf{a}, \mathbf{b})$ is called a *joint maneuver* (n-maneuver or simply maneuver when there is no ambiguity) for the n-aircraft system. A joint maneuver $\alpha = (\alpha_1, \ldots, \alpha_n) \in \mathbf{P}(\mathbf{a}, \mathbf{b})$ is said to be *conflict-free* if for all the duration of the encounter, none of the aircraft enters the cylindrical protection zone of radius R and height $2H$ surrounding another aircraft, or equivalently, there does not exist a pair of indices (i, j) with $1 \leq i < j \leq n$ such that $\|\alpha_{i,xy}(t) - \alpha_{j,xy}(t)\| < R$ and $|\alpha_{i,z}(t) - \alpha_{j,z}(t)| < H$ for some $t \in T$. Here we use the notations that for a given $c \in \mathbf{R}^3$, c_{xy} and c_z are the components of c on the horizontal xy plane and the vertical z-axis respectively.

We denote with $\mathbf{P}(R, H; \mathbf{a}, \mathbf{b})$ the set of all *conflict-free (joint) maneuvers* with starting position $\mathbf{a} = (a_1, \ldots, a_n)$ and destination position $\mathbf{b} = (b_1, \ldots, b_n)$ for the n-aircraft system. Throughout the paper we assume that each pair of points in the set of starting positions $\{a_1, \ldots, a_n\}$ satisfies either the horizontal or the vertical separation condition so that there is no conflict for the n-aircraft system at time t_0. Similarly for $\{b_1, \ldots, b_n\}$. As a result, the set $\mathbf{P}(R, H; \mathbf{a}, \mathbf{b})$ is nonempty.

he performance of each n-maneuver $\alpha \in \mathbf{P}(\mathbf{a}, \mathbf{b})$ can be characterized in term of its *μ-energy* defined by

$$J_\mu(\alpha) = \sum_{i=1}^{n} \mu_i J(\alpha_i), \tag{4.2}$$

where $J(\alpha_i)$ is the energy of α_i defined in equation (4.1), and $\mu_1, \ldots, \mu_n$ are positive real numbers adding up to 1 that represent the priorities of the aircraft. Without the separation constraint, the μ-energy minimizing joint maneuver is clearly the one in which each aircraft fly at constant speed along a straight line. If we restrict our attention to conflict-free joint maneuvers, the ones with smaller μ-energy will still tend to be straighter and smoother, which has practical implications in terms of passenger comfort and fuel consumption. Moreover, by an appropriate choice of the coefficients $\{\mu_i\}$, we can assign different priorities to the aircraft. For example, those aircraft with higher maneuverability can be assigned smaller μ so that they assume a larger responsibility in resolving the conflict.

We say that a conflict-free joint maneuver is the *optimal (resolution) maneuver* for a

multi-aircraft encounter if it is the solution to the following constrained optimization problem:

$$\text{Minimize } J_\mu(\alpha) \text{ subject to } \alpha \in \mathbf{P}(R, H; \mathbf{a}, \mathbf{b}). \tag{4.3}$$

It can be expected that in this formulation, the optimal resolution maneuvers will mainly utilize the vertical dimension for almost all encounters since H is much smaller than R. However, vertical maneuvers are usually the least comfortable ones for passengers. This is the reason why we redefine the energy of a maneuver α_i in equation (4.1) as follows:

$$J(\alpha_i) = \frac{1}{2}\int_{t_0}^{t_f} [\|\dot{\alpha}_{i,xy}(t)\|^2 + \eta^2 |\dot{\alpha}_{i,z}(t)|^2]\, dt, \tag{4.4}$$

where $\eta \geq 1$ is a coefficient introduced to penalize vertical maneuvers. The μ-energy of a joint maneuver α is then defined by (4.2) with $J(\alpha_i)$ given by (4.4) instead of (4.1). This modification does not add further difficulties to the solution of problem (4:3), since the minimization of the new cost function can be easily reduced to the previous one without penalty by scaling the z-axis by a factor of η. The μ-energy with penalty η of a joint maneuver is in fact equal to the μ-energy without penalty of the scaled version of the same joint maneuver, and optimal solutions to the scaled problem can be scaled back to give the optimal solutions to the original problem.

After scaling, the protection zone becomes a cylinder of radius R and height $2\eta H$, hence horizontal resolution maneuvers are more likely to be invoked. In particular, in the level flight case, if $\eta \to \infty$ the problem degenerates into the 2D resolution problem studied in [8].

Without loss of generality, in the following development we then assume $\eta = 1$. A necessary condition for a conflict-free joint maneuver to be optimal is presented in [7]

4.2 Optimal maneuvers for two aircraft encounters

Assume that $\mathbf{a} = (a_1, a_2)$ and $\mathbf{b} = (b_1, b_2)$ are μ-aligned and denote with c their common μ-centroid, i.e., $c = \mu_1 a_1 + \mu_2 a_2 = \mu_1 b_1 + \mu_2 b_2$. An optimal 2-maneuver $\alpha^* = (\alpha_1^*, \alpha_2^*) \in \mathbf{P}(R, H; \mathbf{a}, \mathbf{b})$ satisfies

$$\alpha_1^*(t) - c = -\frac{\mu_2}{\mu_1}(\alpha_2^*(t) - c), \quad \forall t \in T, \tag{4.5}$$

from which it easily follows that the energies of α_1^* and α_2^* are related by $\mu_1^2 J(\alpha_1^*) = \mu_2^2 J(\alpha_2^*)$. Since we need only to search among conflict-free maneuvers satisfying equation (4.5) for α^*, minimizing the μ-energy of the joint maneuver is equivalent to minimizing the energy of the maneuver for a single aircraft, say, aircraft 1.

The separation constraint can be simplified as well, since equation (4.5) implies that it is equivalent to the condition that the curve $\alpha_1^*(\cdot)$ never enters the cylinder W_μ of radius $R_\mu = \mu_2 R$ and height $2H_\mu = 2\mu_2 H$ centered symmetrically around the μ-centroid c. As a result of these simplifications, problem (4.3) is now equivalent to:

$$\text{Minimize } J(\alpha_1) \text{ subject to } \alpha_1 \in \mathbf{P}_1, \text{ and } \alpha_1(t) \notin W_\mu \text{ for all } t \in T, \tag{4.6}$$

which consists in finding minimum energy maneuvers of a single aircraft in the presence of a static obstacle W_μ.

From the discussions following the definition (4.1) of energy of a maneuver, we know that a solution to problem (4.6) is a constant-speed motions along a shortest curve joining a_1 to b_1 while avoiding the obstacle W_μ. Under the feasibility assumption, both a_1 and b_1 belong to $\mathbf{R}^3 \setminus W_\mu$, and such a curve can be computed efficiently. Once α_1^* is computed, α_2^* can be obtained from α_1^* through equation (4.5). This concludes the μ-aligned case.

For the general case when $\mathbf{a}$ and $\mathbf{b}$ are not necessarily μ-aligned, an optimal solution $\alpha^* \in \mathbf{P}(R, H; \mathbf{a}, \mathbf{b})$ to problem (4.3) is given by:

$$\begin{cases} \alpha_1^*(t) = \gamma_1^*(\mathbf{a}, \mathbf{b}+w)(t) - \frac{t-t_0}{t_f-t_0} w \\ \alpha_2^*(t) = \gamma_2^*(\mathbf{a}, \mathbf{b}+w)(t) - \frac{t-t_0}{t_f-t_0} w \end{cases}, \quad \forall t \in T, \tag{4.7}$$

where $(\gamma_1^*(\mathbf{a}, \mathbf{b}+w), \gamma_2^*(\mathbf{a}, \mathbf{b}+w))$ denotes an optimal maneuver in $\mathbf{P}(R, H; \mathbf{a}, \mathbf{b}+w)$ with $w = \mu_1 a_1 - \mu_1 b_1 + \mu_2 a_2 - \mu_2 b_2$.

The optimal solutions depend on the choice of the priority coefficients μ_1 and μ_2. Consider the case when the priority of aircraft 1 is much larger than that of aircraft 2 so that $\mu_2 \simeq 0$. In the μ-aligned case this implies that $a_1 \simeq b_1$, and the radius and height of the cylinder W_μ are approximately 0. Therefore γ_1^* is nearly a zero motion. For general $\mathbf{a}$ and $\mathbf{b}$ that are not necessarily μ-aligned, it follows from the first equation in (4.7) that optimal maneuvers for aircraft 1 are almost constant-speed motions along the line segment from a_1 to b_1. Hence as expected, aircraft 1 behaves as if there were no other aircraft flying in the same region, whereas aircraft 2 is the one assuming the responsibility of avoiding conflicts.

4.3 Some examples of optimal 2-maneuvers

In this section, we present some examples of two-aircraft encounters, and discuss the influence of various factors on the corresponding optimal resolution maneuvers. In all the examples, the coordinates of the aircraft positions are measured in nmi, with $R = 5$ nmi and $H = 0.3292$ nmi.

We start by considering a two-aircraft encounter where $a_1 = (0, 20, 1)$, $b_1 = (40, 20, 1)$, and $a_2 = (20, 0, 1)$, $b_2 = (20, 40, 1)$, so that the straight lines connecting the starting and destination positions of the two aircraft respectively are on the same horizontal plane and cross each other at a right angle.

Figure 4.1 shows an optimal maneuver in the case when the two aircraft have the same priority ($\mu_1 = \mu_2 = 0.5$) and $\eta = 5$. Starting and destination positions of the two aircraft are marked with stars and diamonds respectively, whereas the circles represent the aircraft positions at equally spaced time instants. Hence the denser the circles, the slower the motions. The top view in (b) shows that the conflict is resolved by vertical deviations from the *ideal trajectories*, which are defined to be the constant-speed motions along the straight lines joining starting and destination positions of the two aircraft respectively.

We now study the effect of the priority coefficients on the optimal resolution maneuvers. Plotted in Figure 4.2 are optimal resolution maneuvers for the same two-aircraft orthogonal encounter under three different sets of aircraft priorities and the same η ($\eta = 5$). Although the optimal maneuvers in all three cases have the same top view (shown in the right-hand-side of Figure 4.1), the vertical deviation of aircraft 1 from its ideal trajectory decreases

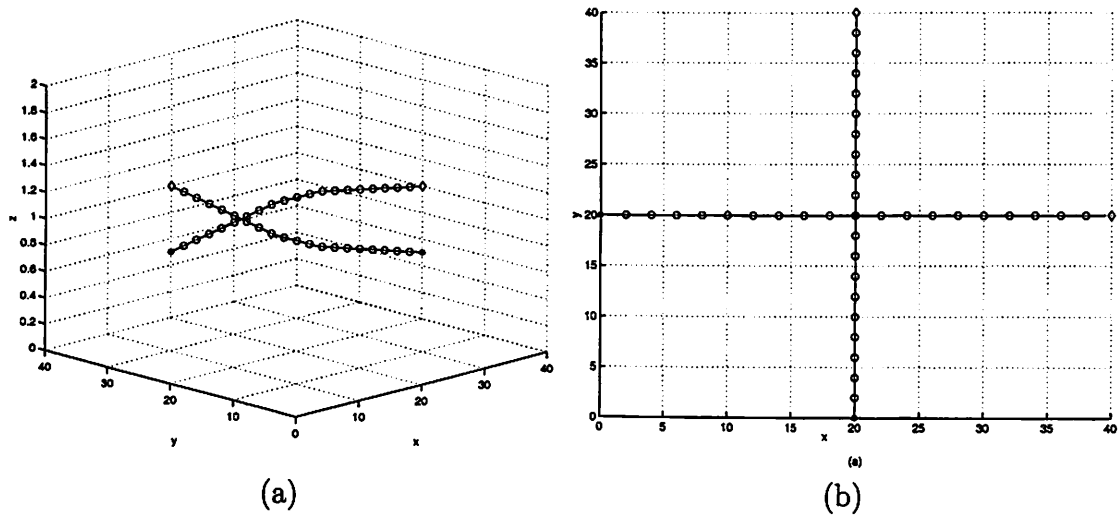

(a) (b)

Figure 4.1: An optimal resolution maneuver for an orthogonal two-aircraft encounter ($\eta = 5$ and $\mu_1 = \mu_2 = 0.5$): (a) three dimensional view; (b) top view.

as its priority increases. In other words, aircraft 2 with smaller priority will assume more responsibility in resolving the conflict. In the extreme case when $\mu_1 = 1$ and $\mu_2 = 0$, the optimal resolution maneuver will be such that aircraft 1 flies along its ideal trajectory, while aircraft 2 assumes all the responsibility of avoiding conflicts with aircraft 1. These conclusions hold in general for two-aircraft and multi-aircraft encounters.

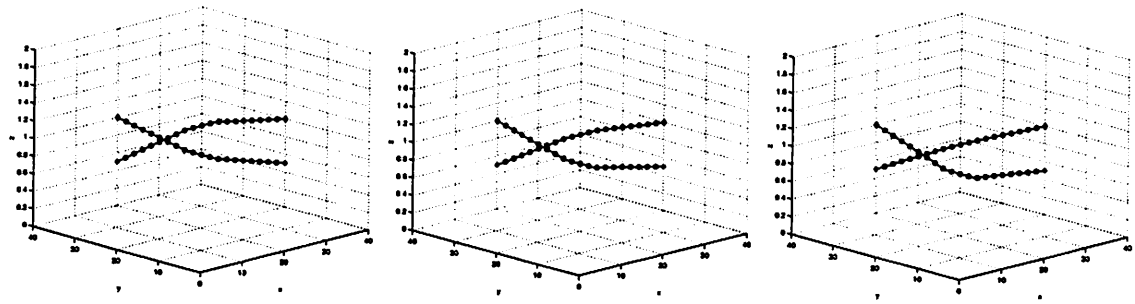

(a) (b) (c)

Figure 4.2: Optimal resolution maneuvers for the orthogonal two-aircraft encounter under three different sets of aircraft priority ($\eta = 5$): (a) $\mu_1 = 0.5$, $\mu_2 = 0.5$; (b) $\mu_1 = 0.7$, $\mu_2 = 0.3$; (c) $\mu_1 = 0.9$, $\mu_2 = 0.1$.

As for the effect of the vertical penalty factor, note that in Figure 4.1 where $\eta = 5$ and $\mu_1 = \mu_2 = 0.5$, the conflict is resolved using only vertical deviations from the ideal trajectories. In contrast, in the case shown in Figure 4.3 where η is set equal to 15 ($\mu_1 = \mu_2 = 0.5$), the conflict is resolved using only horizontal deviations. The explanation is that in order to obtain the optimal resolution maneuvers, we have to scale the z-axis by a factor of η. When η is large so that the height of the cylindrical obstacle becomes much larger than its radius, a shortest curve between two points across the cylinder is more likely to be a curve

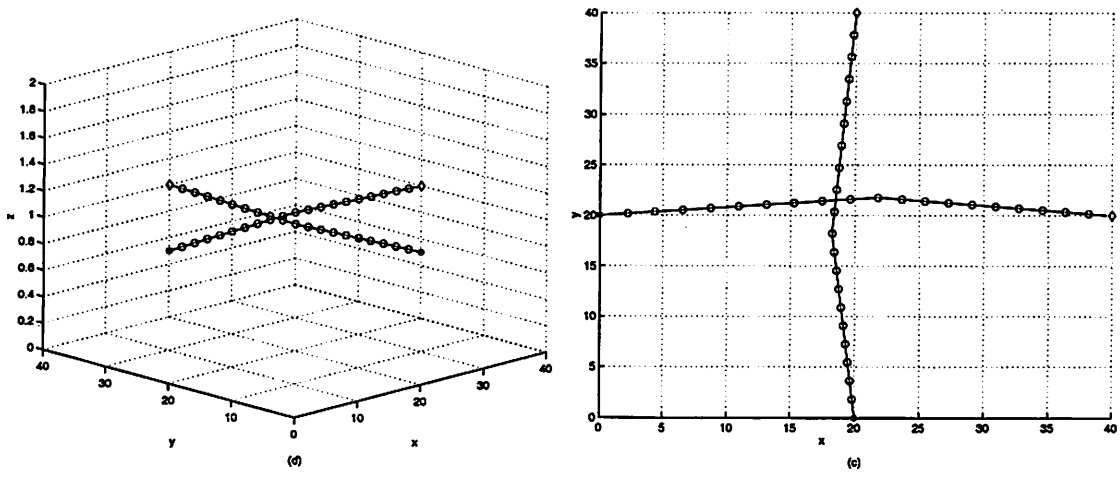

(a) (b)

Figure 4.3: An optimal resolution maneuver for the orthogonal two-aircraft encounter with larger η ($\eta = 15$ and $\mu_1 = \mu_2 = 0.5$): (a) three dimensional view; (b) top view.

around the side of the cylinder rather than around its top or bottom. Therefore the larger the vertical penalty factor η, the more likely it is that an optimal resolution maneuver will consist of horizontal deviations from ideal trajectories. In general, for encounters involving two or more than two aircraft, there are two extreme cases: When η is very large and the aircraft initial and destination positions are all at about the same altitude, the problem degenerates into a planar conflict resolution problem, where only horizontal deviations are allowed in resolving the conflict; When η is close to 0, then only vertical deviations are used in the optimal resolution maneuvers and their top views consist of straight line segments.

It is worth noticing that due to the cylindrical shape of the obstacle, a slight change of starting or destination positions of either aircraft may lead to radically different optimal resolution maneuvers. Take for example the optimal maneuvers for the two-aircraft encounters shown in Figure 4.4, where $a_1 = (0, 20, 1)$, $b_1 = (40, 20, 1)$, $b_2 = (40, 30, 1.2)$ are fixed, and a_2 takes two different values: $a_2 = (0, 10, 0.8)$ shown in (a) and (b) of Figure 4.4, and $a_2 = (0, 11, 0.8)$ shown in (c) and (d) of the same figure. Although the values of a_2 are close in the two cases, the optimal resolution maneuvers look quite different. While both consisting of three constant-speed motions along straight line, the optimal maneuver in the first case experiences more dramatic altitude changes in the early stage than in the late stage, while the situation is reversed in the second case.

4.4 Optimal two-legged maneuvers for multiple aircraft encounters

4.4.1 Reformulation of the problem

Consider an n-aircraft system with starting position $\mathbf{a} = (a_1, \ldots, a_n)$ and destination position $\mathbf{b} = (b_1, \ldots, b_n)$. Fix an epoch $t_c \in T$ such that $t_0 < t_c < t_f$. For each aircraft i, $i = 1, \ldots, n$,

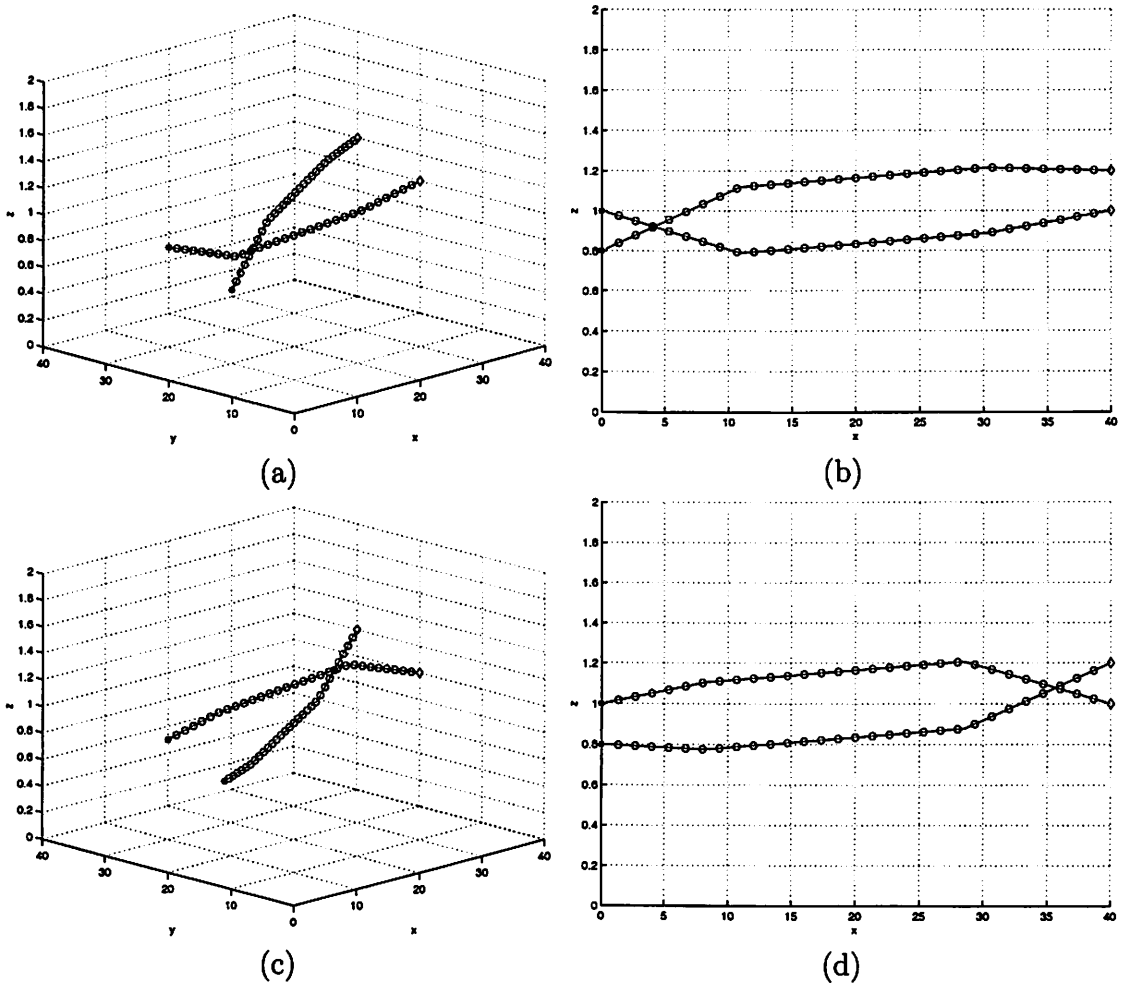

Figure 4.4: Optimal resolution maneuvers for two-aircraft encounters with the same a_1, b_1, b_2 and two different values of a_2 ($\eta = 5$ and $\mu_1 = \mu_2 = 0.5$): (a) three dimensional view and (b) projection onto the xz-plane for the case $a_2 = (0, 10, 0.8)$; (c) three dimensional view and (d) projection onto the xz-plane for the case $a_2 = (0, 11, 0.8)$.

choose a way point $c_i \in \mathbf{R}^3$. Then a *two-legged maneuver* with way point c_i for aircraft i is a maneuver consisting of two stages: first from a_i at time t_0 to c_i at time t_c, and then from c_i at time t_c to b_i at time t_f, moving at constant velocity in both stages. Denote with $\mathbf{P}_{i,2}$ the set of all two-legged maneuvers of aircraft i, and with $\mathbf{P}_2(\mathbf{a}, \mathbf{b}) = \prod_{i=1}^n \mathbf{P}_{i,2}$ the set of all *two-legged joint maneuvers* of the n-aircraft system. Denote with $\mathbf{P}_2(R, H; \mathbf{a}, \mathbf{b})$ the subset of $\mathbf{P}_2(\mathbf{a}, \mathbf{b})$ consisting of all those elements of $\mathbf{P}_2(\mathbf{a}, \mathbf{b})$ that are conflict-free. We assume that the epoch t_c is fixed throughout this section, so that each maneuver in $\mathbf{P}_2(\mathbf{a}, \mathbf{b})$ (and hence in $\mathbf{P}_2(R, H; \mathbf{a}, \mathbf{b})$) is uniquely specified by the way points $(c_1, \ldots, c_n)$.

In this section we shall try to solve the following problem:

$$\text{Minimize } J_\mu(\alpha) \text{ subject to } \alpha \in \mathbf{P}_2(R, H; \mathbf{a}, \mathbf{b}). \tag{4.8}$$

The reason for studying problem (4.8) instead of the general problem (4.3) is that in the

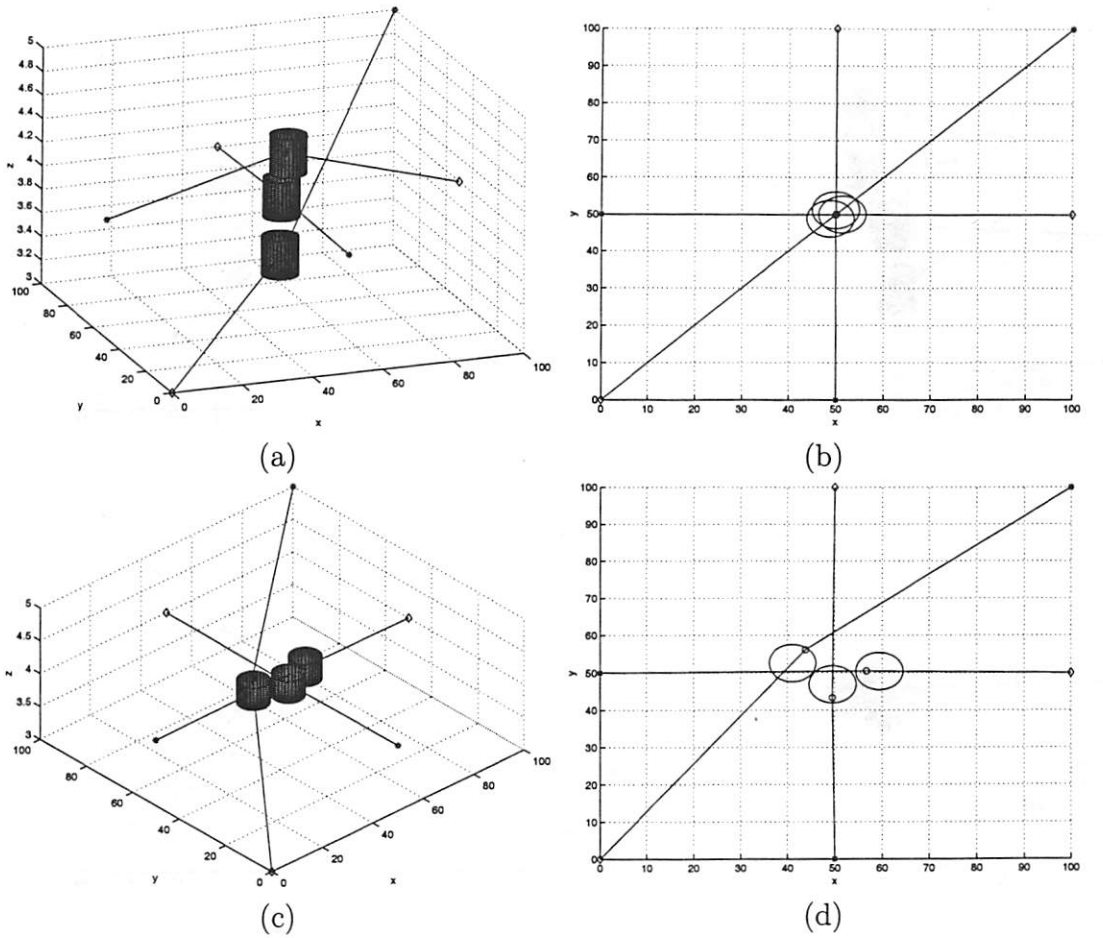

Figure 4.5: Two-legged resolution maneuvers for a three-aircraft encounter ($\mu_1 = \mu_2 = \mu_3 = 1/3$): (a) three dimensional view and (b) top view in the case $\eta = 5$; (c) three dimensional view and (d) top view in the case $\eta = 50$.

ATM practice, it is simpler for the central controller to transmit the aircraft trajectory information in the form of way points and time to reach these way points rather than continuous trajectories. From a methodological point of view, since each maneuver in $\mathbf{P}_2(R, H; \mathbf{a}, \mathbf{b})$ is parameterized by a way points vector $(c_1, \ldots, c_n)$, which resides in a finite dimensional vector space, problem (4.8) is a finite dimensional optimization problem, which is much easier to deal with than the variational problem (4.3).

4.4.2 Some examples of multi-aircraft encounters

Consider a three-aircraft encounter where $a_1 = (0, 50, 4)$, $b_1 = (100, 50, 4)$, $a_2 = (50, 0, 4)$, $b_2 = (50, 100, 4)$, $a_3 = (100, 100, 5)$, and $b_3 = (0, 0, 3)$, i.e., aircraft 1 and aircraft 2 are flying at the same altitude with cross-path angle of 90°, whereas aircraft 3 dives across that altitude and has a path angle of 135° with both aircraft 1 and aircraft 2. All the three aircraft have identical priority and $t_c = (t_0 + t_f)/2$. We choose a larger R ($R = 10$ nmi) to make the resolution maneuvers more evident. In Figure 4.5 the solutions to problem in section 4.4.1.

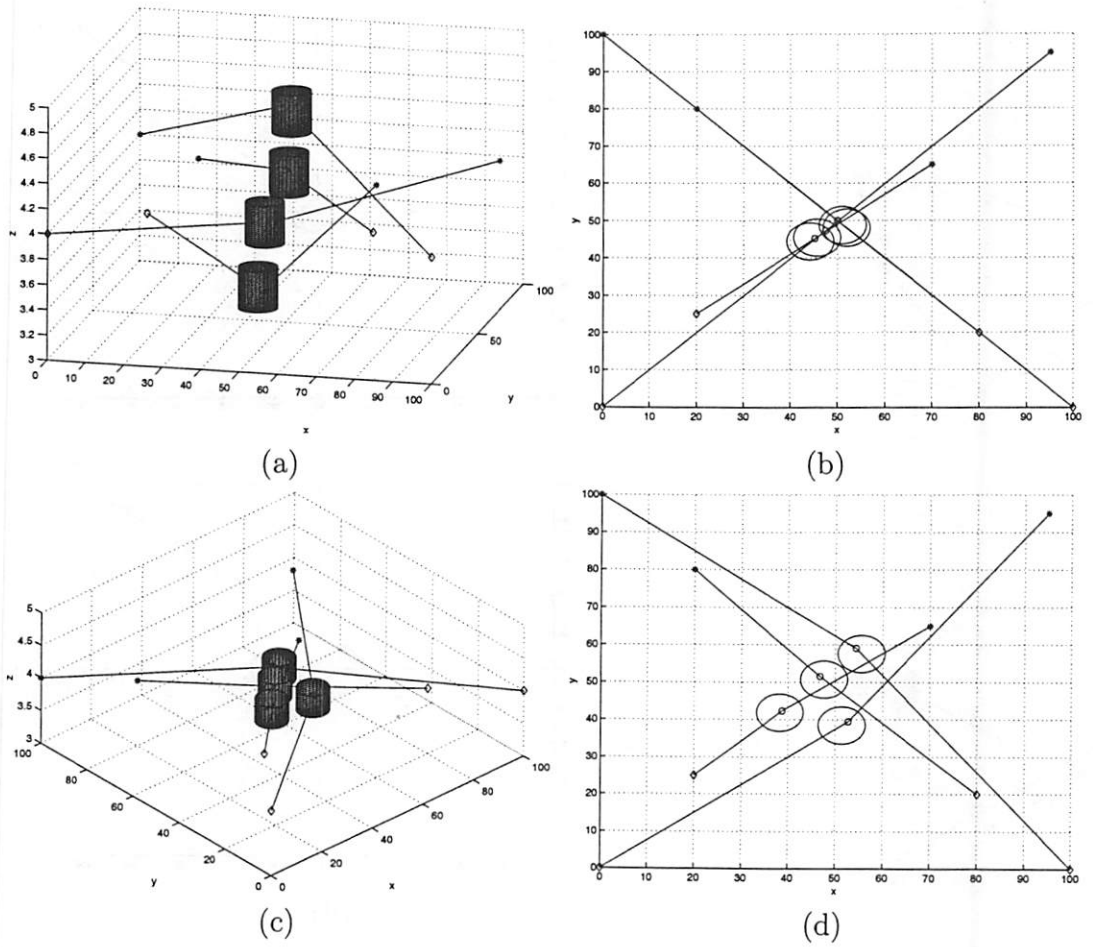

Figure 4.6: Two-legged resolution maneuvers for a four-aircraft encounter ($\mu_1 = \mu_2 = \mu_3 = \mu_4 = 1/4$): (a) three dimensional view and (b) top view in the case $\eta = 5$; (c) three dimensional view and (d) top view in the case $\eta = 50$.

corresponding to two different values of η are shown. Plotted in (a) is the snapshot at a time instant near t_c of the two-legged joint maneuver that is a solution to problem (4.8) with $\eta = 5$. Its top view is shown in (b). The cylinders in (a) represent *half* the size of the protection zones surrounding each aircraft, i.e., cylinders of radius $R/2$ and height H. Therefore two aircraft are in a conflict situation if and only if the corresponding cylinders intersect each other. Similarly, (c) and (d) plot a snapshot of the solution to problem (4.8) with $\eta = 50$. As in the case of two-aircraft encounters, larger value of η will force the aircraft to adopt horizontal maneuvers to resolve the conflict.

Figure 4.6 shows the simulation results for a four-aircraft encounter with $a_1 = (0, 100, 4)$, $b_1 = (100, 0, 4)$, $a_2 = (20, 80, 4)$, $b_2 = (80, 20, 4)$, $a_3 = (95, 95, 4)$, $b_3 = (0, 0, 4)$, $a_4 = (70, 65, 4)$, and $b_4 = (20, 25, 4)$. The four aircraft are divided into two groups, each consisting of two aircraft one overtaking the other, with the path angle between the two groups being 90°. We choose $R = 10$ nmi, $H = 0.3292$ nmi, and $t_c = (t_0 + t_f)/2$. All aircraft have equal priority. (a) and (b) plot the snap shot of the solution at a time instant near t_c when $\eta = 5$,

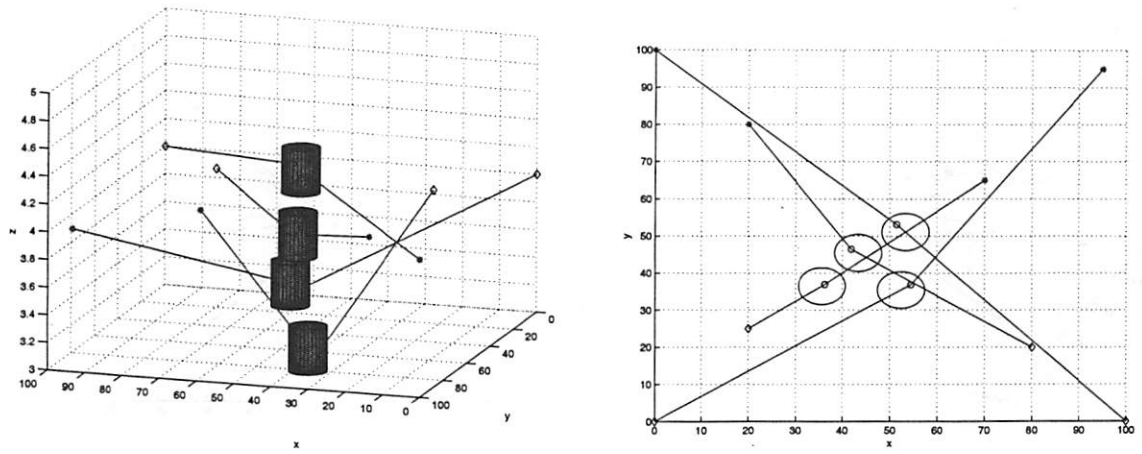

(a) (b)

Figure 4.7: Two-legged resolution maneuvers for the four-aircraft encounter ($\mu_1 = 0.7$, $\mu_2 = \mu_3 = \mu_4 = 0.1$): (a) three dimensional view in the case $\eta = 5$ and (b) top view in the case $\eta = 50$.

(c) and (d) plot a snapshot of the solution when $\eta = 50$. (c) and (d) can be thought of as the restricted solution to problem (4.8) when the motion of each aircraft is required to be contained in the plane of altitude 4. If we increase the priority of aircraft 1 such that $\mu_1 = 0.7$, $\mu_2 = \mu_3 = \mu_4 = 0.1$, we obtain the results shown in (a) and (b) of Figure 4.7 for $\eta = 5$ and $\eta = 50$ respectively. Compared with (a) and (d) of Figure 4.6, we can see that the motions of aircraft 1 are closer to the straight line motions, forcing other aircraft to "bend" more.

When the number of aircraft involved gets larger, the resolution maneuver becomes more complicated. An example is shown in Figure 4.8 for an eight-aircraft encounter, which is obtained by adding to the four-aircraft encounter in Figures 4.6 and 4.7 four more aircraft with $a_5 = (55, 0, 3.7)$, $b_5 = (50, 80, 3.7)$, $a_6 = (55, 20, 3.7)$, $b_6 = (50, 100, 3.7)$, $a_7 = (0, 55, 3.7)$, $b_7 = (80, 45, 4)$, $a_8 = (20, 55, 3.7)$, and $b_8 = (100, 45, 4)$. By choosing identical priority and $\eta = 20$, the obtained solution to problem consists of both horizontal and vertical resolution motions. (a), (b) and (c) are views of the solution from different viewpoints, (d) is its snapshot at a certain time instant.

4.4.3 Constraints on the velocity and the turning angle for the aircraft maneuver feasibility

So far we have assumed that the two-legged maneuver obtained by solving the optimization problem (Section 4.4.1) is flyable. In practice, this is usually not the case because of the abrupt turn and the change of speed when an aircraft passes through its way-point. In the following we shall propose practical constraints on the way-points to alleviate such drawbacks, at least to a certain extent. In order for the optimization problem to be computationally tractable, it is important that the introduced constraints be convex.

We start by considering the speed constraint: the speed of each aircraft during both

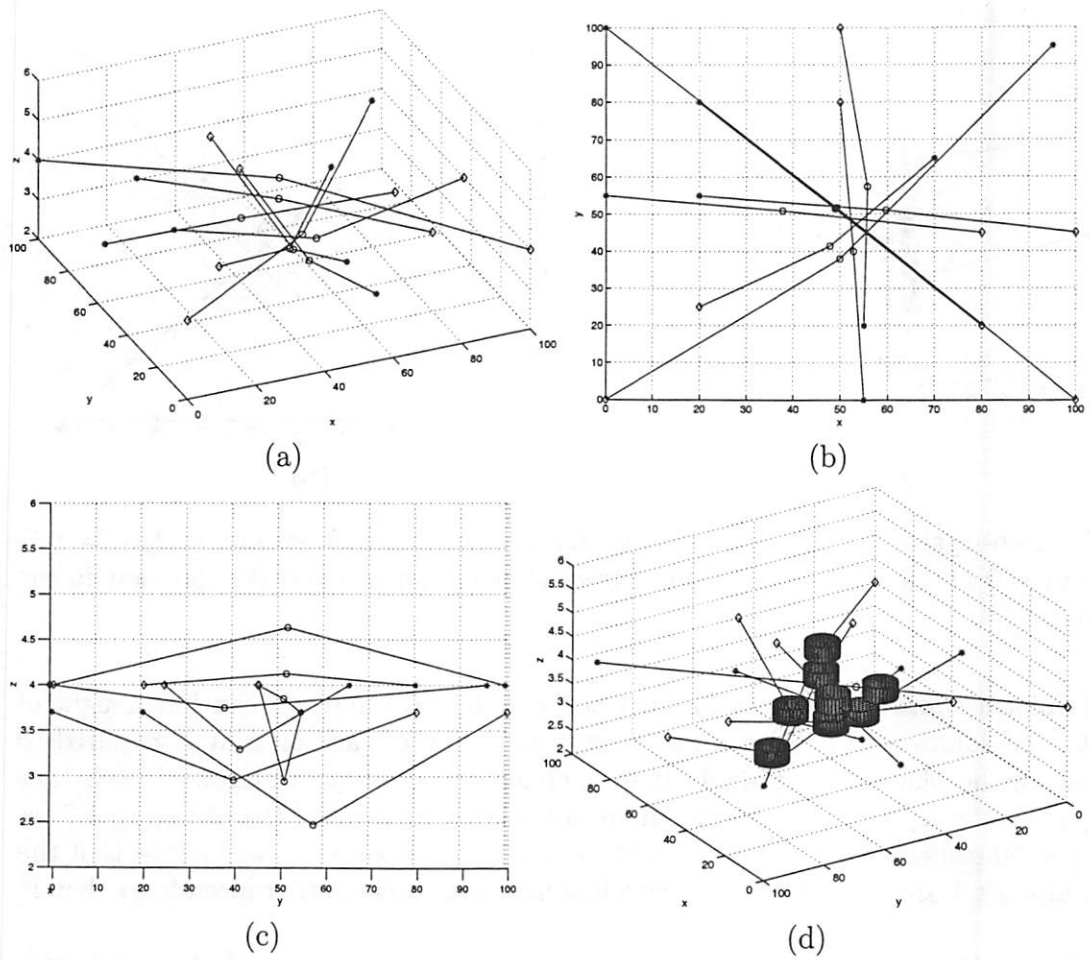

Figure 4.8: Two-legged maneuvers for an eight-aircraft encounter ($\mu_i = 1/8$, $i = 1, \ldots, 8$, $\eta = 20$).

stages of its motion cannot exceed a certain threshold v_{max}. Recall that t_c is the time epoch corresponding to the middle way-points c_i's. Then the speed constraint can be expressed as:

$$\|a_i - c_i\| \leq v_{max}(t_c - t_0), \quad \|b_i - c_i\| \leq v_{max}(t_f - t_c), \quad i = 1, \ldots, n. \tag{4.9}$$

For a single aircraft, say aircraft i, constraint (4.9) implies that c_i must belong to the intersection of two spheres, one centered at a_i and the other centered at b_i. Hence the speed constraint is convex. Instead of a common v_{max}, one can also impose different speed upper bounds for the aircraft.

A further practical constraint is the turning angle constraint: the angle each aircraft turns at its way-point cannot exceed a certain threshold θ_{max}. For aircraft i, this constraint specifies that its way-point c_i must lie in a convex region of $\mathbf{R}^3$ that is invariant under rotation around the axis $\overline{a_i b_i}$, which is the straight line passing through a_i and b_i. The intersection of this convex region with any plane through $\overline{a_i b_i}$ is plotted in Figure 4.9. It is the intersection of two disks with properly chosen centers and radii.

Note that each one of the two constraints above can be expressed using the *second order*

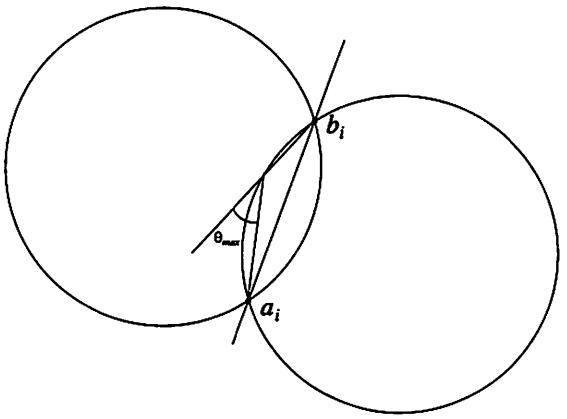

Figure 4.9: Turning angle constraint on way-points.

cone constraints of the form (assume s is the optimization variable)

$$\|\hat{A}s + \hat{b}\| \leq \hat{c}s + \hat{d}, \tag{4.10}$$

for some matrix $\hat{A}$, vectors $\hat{b}$, $\hat{c}$ and constant $\hat{d}$ of suitable dimensions. Although the turning angle constraint is actually equivalent to an infinite number of second order cone constraints, one can, for example, impose an upper bound on the turning angle for the projections of the maneuver onto the plane xy, xz and yz respectively, thus leading to three second order cone constraints. Therefore, the optimization problem in section 4.4.1 together with the speed and the simplified turning angle constraints become a Second Order Cone Programming (SOCP), which can be solved using softwares such as SOCP ([15]). Note that as before, the vertical discount factor η can be incorporated into these two constraints.

Figure 4.10 shows the effect of the speed and turning angle constraints by considering a five-aircraft encounter. The solution to problem in sction 4.4.1 without any additional constraint is shown in (a), the solution with the speed constraint of $v_{max} = 7.102$ nmi/min is shown in (b), whereas the solution with the turning angle constraint $\theta_{max} = \pi/10$ on the xy plane projection is plotted in (c). Here we choose $t_0 = 0$ min, $t_f = 10$ min, $t_c = 5$ min, $\eta = 50$, $R = 5$ nmi, and all aircraft have identical priority. It can be seen that, as expected, the aircraft with the largest speed and turning angle (the one starts from the top left corner and ends in the bottom right corner) tends to have a straighter motion under the added constraints on either the speed or the turning angle.

Further adjustments can be introduced to improve the flyability of the generated maneuvers. For example, one can consider multi-legged maneuvers and adopt an iterative procedure to get an approximated optimal solution for the multi-legged version of the conflict resolution problem. Also, to avoid the sharp turns that the generated maneuvers may cause for the aircraft at time t_0, one can choose the starting epoch to be $t_0 + \Delta$ for some positive Δ, and use the time interval $[t_0, t_0 + \Delta]$ as the buffer for possible heading adjustments. It should be pointed out that the effort in this chapter is only a small step towards the implementation of our algorithm in practical situations, and much more work needs to be done in this aspect.

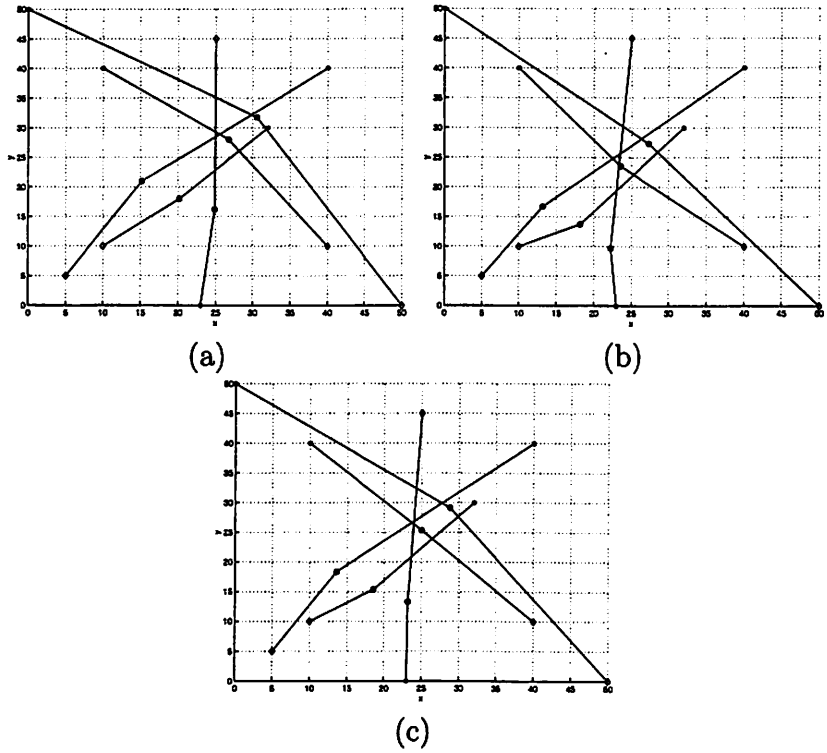

Figure 4.10: Two-legged resolution maneuvers for a five-aircraft encounter ($\mu_1 = \mu_2 = \mu_3 = \mu_4 = 1/4$, $\eta = 50$): (a) no additional constraint; (b) speed constraint with $v_{max} = 7.102$ nmi/min; (c) turning angle constraint with $\theta_{max} = \pi/10$.

Chapter 5

Conclusions and Future work

We presented a stochastic algorithm to detect mid-range aircraft conflict. Monte-Carlo simulation is performed to validate our detection model. There is an explicit separation between the probabilistic model used for our prediction and validation. In the validation scheme, our method shows a drastically improved ratio of conflicts detected per false alarm. Our validation scheme also provides appropriate value for the various design parameters such as the threshold conflict probability which can be successfully utilized in order to increase the performance of the ATC system. Moreover, in our approach, we have used randomized algorithms to manage the computational complexity of the problem and to provide quantitative estimates of the level of approximation involved.

We studied the resolution algorithm when multiple aircraft are involved in a potential conflict. First, we proposed an algorithm for the two dimensional case. Consequently, we have presented the extension of the algorithm for the three dimensional case. A randomized algorithm is used in order to know the type of the resolution maneuver and an optimization is carried out where the type of the resolution maneuver is known from the randomized algorithm. The original optimization algorithm is approximated by a convex optimization problem by considering two legged maneuvers and the linear approximation of the feasible region. The feasibility of the flight plan is also taken into account by introducing maximum speed and the turning angle constraints.

The algorithms presented here work in the tactical level. The direction of our future research work will lead us to the strategic level. The transition is inherently dependent on a seemless and efficient interface between the two. One example can be cited in the case of aircraft conflict resolution, as it applies to the avoidance of bad weather. In the current system, a major portion of the delay is due to bad weather. A strategic level algorithm is required to reroute the aircraft in order to reduce weather related delay. As the aircraft approaches the site of the bad weather, the strategic conflict avoidance transitions into a tactical one. Here, the conflict detection and resolution schemes that we have presented can be applied to develop an efficient rerouting of the aircraft if it is integrated well with the strategic detection and resolution schemes.

The development of a safe and efficient National Airspace System (NAS) is dependent upon strategic and tactical conflict detection and resolution schemes which are well integrated. It is the intention of this author to pursue this union in the hopes of creating a much improved ATC system.

Bibliography

[1] D. Bertsimas and Stock Patterson. The air traffic flow problem with enroute capacities. *Operations Research*, 46:406–422, 1998.

[2] S. Boyd. *Convex Optimization.* Course reader for EECS 290N, University of California, Berkeley, California, Fall, 1999.

[3] N. Durand, J.M. Alliot, and J. Noailles. Automatic aircraft conflict resolution using genetic algorithm. In *11th annual ACM Conference on applied computing*, Philadelphia, USA, 1996.

[4] Heinz Erzberger and Russell A. Paielli. Conflict probability and estimation for the free flight. In *In Proc.35th Meeting, AIAA-97-0001*, 1997.

[5] Radio Technical Commission for Aeronautics. Minimum aviation system performance standards for automatic dependent surveillance-broadcast. Technical report, RTCA 186, DRAFT 4.0, 1997.

[6] E. Frazzoli, Z.H. Mao, and E. Feron. Resolution of conflicts involving many aircraft via semidefinite programming. *Preprint*, 1999.

[7] J. Hu, M. Prandini, A. Nilim, and S. Sastry. Three dimensional coordinated maneuvers for aircraft conflict avoidance. In *AIAA Guidance, Navigation and Control Conference (submitted)*, 2001.

[8] J. Hu, M. Prandini, and S. Sastry. Optical coordinated maneuver for multiple agent moving on a plane. 2000. (preprint).

[9] J. Hu, M. Prandini, and S. Sastry. Optimal maneuver for multiple aircraft conflict resolution: a braid point of view. In *Proc. 39th CDC*, Sidney, Australia, 2000.

[10] Jianghai Hu. A study of conflict detection and resolution in free flight. Master's thesis, University of California, Berkeley, 2000.

[11] J. Kuchar and L.C. yang. Survey of conflict detection and resolution modeling methods. In *AIAA Guidance, Navigation, and control Conference*, New Orleans, Louisiana, 1997.

[12] J. Kuchar and L.C. yang. Prototype conflict alerting logic for free flight. In *In Proc.35th AIAA Airspace Science Meeting and Exhibit, AIAA 97-0220*, January, 1997.

[13] James K. Kuchar. *A Unified Methodology for the Evaluation of Hazard Alerting Systems.* PhD thesis, Massachusetts Institute of Technology, 1995.

[14] J. Lygeros and N. Lynch. On the formal verification of the tcas conflict resolution and algorithms. In *In Proc. 36th IEEE Conference on Decision and Control*, San Diego, USA, 1997.

[15] M.Molo, L. Vandenberghe, S. Boyd, and H. Lerbet. Application of second-order cone programming. *Linear Algebra and its Applications*, 284(1-3):193–228, 1998.

[16] Russell A. Paielli and Heinz Erzberger. Conflict probability estimation for free flight. *Journal of Guidance, Control and Dynamics*, 20(3):588–596, 1997.

[17] M. Prandini, J. Lygeros, A. Nilim, and S. Sastry. A probabilistic framework for aircraft conflict detection. In *Proc. AIAA Guidance, Navigation and Control Conf*, Portland, Oregon, 1999.

[18] M. Prandini, J. Lygeros, A. Nilim, and S. Sastry. Randomized algorithms for probabilistic aircraft conflict detection. In *Proc. 38th CDC*, Phoenix, Arizona, December,1999.

[19] S. Sastry, G. Meyer, C. Tomlin, J. Lygeros, D. Godbole, and G. Pappas. Hybrid systems in air traffic control. In *IEE Conference on Decision and Control*, pages 1478–1483, New Orleans, Louisiana, 1995.

[20] C. Tomlin, G. Pappas, and S. Sastry. Conflict resolution for air traffic management: a study in multi-agent hybrid systems. *IEEE Transaction of automatic control*, 43:509–521, 1998.

[21] Claire Tomlin. *Hybrid control of air traffic management system.* PhD thesis, University of California, Berkeley, 1997.

[22] M. Vidyasagar. *A theory of learning and generalization: with applications to neural networks and control systems.* Springer-Verlag, London, 1997.

[23] P.B.M Vranas, D. Bertsimas, and A.R. Odoni. Dynamic ground holding policies for a network of airports. *Transportation Science*, 28:275–291, 1994.